ELSEVIER

Contents lists available at ScienceDirect

Geochimica et Cosmochimica Acta

journal homepage: www.elsevier.com/locate/gca



Halogen enrichment in the North American lithospheric mantle from the dehydration of the Farallon plate



George Segee-Wright ^{a,*}, Jaime D. Barnes ^a, John C. Lassiter ^a, Duncan J. Holmes ^a, Grace M. Beaudoin ^a, Rudra Chatterjee ^a, Daniel F. Stockli ^a, J. Elis Hoffmann ^b, Timm John ^b

ARTICLE INFO

Article history: Received 14 May 2022 Accepted 8 March 2023 Available online 14 March 2023 Associate editor: Janne Blichert-Toft

Keywords: Halogen elements Volatile cycling Mantle xenolith Lithospheric mantle Metasomatism

ABSTRACT

A greater quantity of halogens (F, Cl, Br, and I) appear to be subducted globally than are erupted at magmatic arcs, requiring either an increase in the mantle halogen budget through time or an additional output pathway or reservoir. The sub-continental lithospheric mantle (SCLM) is one such reservoir. SCLM can be enriched in volatile elements after metasomatism by fluids or melts from subducting oceanic lithosphere. We analyzed the bulk halogen content (F, Cl, Br, and I) of 28 variably metasomatized spinel and garnet peridotite xenoliths from the Navajo Volcanic Field (NVF; Central Colorado Plateau) to constrain the effects of the subducting Farallon plate-derived metasomatism on the halogen content of the western North American SCLM. We also analyzed 33 anhydrous spinel peridotites from various localities on and around the Colorado Plateau, as well as xenoliths from Oahu, Hawaii, and Eifel, Germany to compare them to the modally hydrated NVF xenoliths. Cl, Br, and I are enriched in NVF xenoliths relative to the depleted mantle, correlating with olivine oxygen isotope values and indices of metasomatism. F is less enriched, indicating preferential retention in the slab residue. Br/Cl and I/Cl are similar to partially dehydrated serpentinite, indicating that the source of these fluids is consistent with serpentinized oceanic lithosphere of the Farallon plate. Anhydrous xenoliths from the southwestern United States have more depleted mantle-like Cl and F contents but have highly enriched Br contents similar to the NVF xenoliths. Similar to NVF xenoliths, anhydrous xenolith Br/Cl and I/Cl suggest a Farallon derived serpentinite source of halogen enrichment. These results indicate that the Farallon slab sequestered halogens in the North American SCLM of the central and south Colorado Plateau and the southern Rio Grande Rift. Therefore, halogen sequestration in the SCLM may be a critical component in the global halogen cycle. © 2023 Elsevier Ltd. All rights reserved.

1. Introduction

The majority of Earth's halogen budget is contained in the crust and hydrosphere (Sharp and Draper, 2013; Kendrick et al., 2017; Hanley and Koga, 2018), but halogens from these surface reservoirs can be introduced to the mantle via subduction. Subduction of halogens into the mantle affects mineral strength and solidus, altering the overall rheology and melting behavior of mantle minerals (Chu et al., 2011; Filiberto et al., 2012, 2014). Additionally, the balance of halogens subducted into the convecting mantle and erupted to the surface at ridges, arcs, and ocean islands has implications for geochemical evolution of the mantle and the volatile content of Earth's surface (Sharp and Draper, 2013; Kendrick et al., 2017; Broadley et al., 2018; Broadley et al., 2019). However, the fate of subducted halogens remains equivocal. Mass balance calculations indicate that

the global flux of all halogens into subduction zones is greater than the flux to the surface at arcs, requiring either an unsampled halogen flux to the surface or a halogen sink in the mantle or lower crust (Barnes et al., 2018 and references therein; Gibson et al., 2020; Bekaert, et al., 2021). Where these "missing" halogens reside and what subducted lithologies carry them remains uncertain.

A potentially important sink for subducted halogens is intraplate sub-continental lithospheric mantle (SCLM). Because SCLM can remain chemically isolated from the convecting mantle, enrichment of the SCLM can remove halogens from long-term cycling between the surface and convecting mantle. Some previous studies of intra-plate SCLM xenoliths found little to no Cl, Br, and I enrichment and moderate F enrichment resulting from slab-derived metasomatism (Johnson et al., 2000; Urann et al., 2017; Kobayashi et al., 2019), whereas others documented moderate to large enrichments in Cl, Br, and I in metasomatized SCLM (Patiño Douce et al., 2011; Broadley et al., 2016, 2018; Toyama et al., 2021).

^a University of Texas at Austin, Department of Geological Sciences, 1 University Station C1160, Austin, TX 78712-0254, USA

^b Freie Universität Berlin, Institute for Geological Sciences, Malteserstraße 74-100, Gebäude B,C, D, E, N and T 12249, Berlin, Germany

^{*} Corresponding author. E-mail address: ghs562@utexas.edu (G. Segee-Wright).

This study examines the whole-rock F, Cl, Br, and I concentrations and oxygen isotope compositions of olivine mineral separates of intra-plate peridotite xenoliths from various localities in the Colorado Plateau, Basin and Range, and the Rio Grande Rift in the southwestern United States that have experienced variable degrees of subduction-related metasomatism from Farallon plate-derived fluids/melts (e.g. Lee, 2005; Marshall et al., 2017b). We also analyze a suite of oceanic lithospheric mantle peridotite xenoliths from Oahu, Hawaii and metasomatized SCLM peridotite xenoliths from the Eifel volcanic field to compare to the North American SCLM results. We use halogen abundance data for these geochemically well-characterized xenoliths to determine the extent and source of subduction-related metasomatic halogen enrichment in the North American SCLM.

However, other processes such as melt depletion and melt metasomatism can also affect the halogen content of the SCLM, so halogen content alone is not sufficient to demonstrate a subduction-derived source. Instead, a combination of xenolith halogen contents, olivine oxygen isotope ratios, and trace element concentrations provide more robust evidence for the source of halogen enrichment in the lithospheric mantle. Particularly powerful are the ratios of halogens to similarly incompatible lithophile elements (F/Nd, Cl/Nb, Br/Nb, and I/Nb) since these ratios do not vary significantly during typical mantle melting or fractional crystallization (Sun et al., 2007; Kendrick et al., 2017). The invariance of these ratios during most mantle processes allows them to be used to detect halogen enrichment from a subducted source that may alter halogen/lithophile ratios due to preferential mobilization of halogens in aqueous fluids (Manning, 2004).

2. Geologic setting and samples

2.1. North American SCLM

Prior to 80 Ma, the Farallon plate subducted steeply beneath the North American plate but transitioned to shallow-slab subduction between ~80 and 40 Ma, resulting in the Laramide Orogeny (Dickinson and Snyder, 1978; Humphreys et al., 2003, Humphreys, 2009). Dehydration of the Farallon slab released hydrous fluids and melts over a broad region and variably metasomatized the overlying North American SCLM via slab-derived fluids and melts (Fig. 1a; e.g., Lee, 2005). Fluid-mobile element enrichment (Lee, 2005; Rowe and Lassiter, 2009; Rowe et al., 2015; Marshall et al., 2017b), stable isotope ratios (Perkins et al., 2006; Marshall et al., 2017b), and petrologic observations (Smith, 1979; Smith, 1995; Smith, 2010) of North American SCLM xenoliths indicate that Farallon-derived metasomatism extended up to 1000 km from the trench. The mechanism allowing for the retention of hydrous minerals in the Farallon plate at these great distances is uncertain, but is likely related to the fast plate motion (10-15 cm/year; English et al., 2003) of the Farallon plate and its contact with the relatively cool North American SCLM decreasing the conductive heat flow into the subducting Farallon plate. Cooler temperatures of the SCLM in contact with the Farallon plate (Smith, 2010) allowed for hydrous mineral formation and stabilization in the SCLM (Humphreys et al., 2003). Slab removal initiated ~40 Ma and exposed the metasomatized lithospheric mantle to the warmer asthenosphere, triggering voluminous post-Laramide volcanism across the southwestern United States (Lee, 2005).

SCLM peridotite xenoliths analyzed in this study are divided into modally hydrated and anhydrous xenoliths. Sample thin sections were examined, and any samples with signs of surficial alteration, (e.g., sericitization, clay minerals along grain boundaries; see supplementary materials) were discarded.

2.1.1. Modally Hydrated North American Peridotite Xenoliths

We analyzed suites of modally hydrated peridotite xenoliths from the Navajo Volcanic Field (NVF) (n = 28; Fig. 1b) on the central Colorado Plateau. The Colorado Plateau is a relatively thick (120-150 km) and stable block of lithosphere (Gao et al., 2004; West et al., 2004). The Navajo Volcanic Field is in central Colorado Plateau. It has an area of >30,000 km² and is composed of \sim 50 minette necks and ~8 diatreme-forming intrusions called serpentinized ultramafic microbreccias (SUM) (Roden, 1981; Marshall et al., 2017a, 2017b; Smith, 1979, 2010) that formed between 30 and 20 Ma (Laughlin et al., 1986). We examine SUM-hosted xenoliths from two localities in the Navajo Volcanic Field: Green Knobs and Moses Rock (Fig. 1b). SUM diatremes erupted at as solid-gas mixtures (McGetchin et al., 1973; Smith and Levy, 1976) with eruptive temperatures <600-650 °C (Smith, 2013). The SUM are temporally and spatially related to minettes, but the SUM diatremes were not derived from silicate melts (Smith and Levy. 1976) but rather were formed either from the intrusion of minette magmas into the hydrated SCLM (Smith and Levy, 1976) or from exsolution of a CO₂-H₂O fluid as minette magmas intersect the solidus as it rises through the SCLM and cools (Roden, 1981).

The analyzed Navajo Volcanic Field xenoliths are modally hydrated peridotites that were formerly spinel lherzolites and harzburgites, although two samples have chlorite pseudomorphs of garnet (N23-GN and N71-GN; Roden et al., 1990). The xenoliths have been interpreted as Proterozoic SCLM based on Re depletion ages and Sm-Nd dates (Marshall et al., 2017a). NVF xenoliths contain 1-90 modal % amphibole, chlorite, and antigorite with minor clinohumite. Only one sample (N178-GN) has trace amounts of phlogopite. These hydrous mineral assemblages have been interpreted to have formed in the SCLM between 400 and 650 °C due to metasomatism from Farallon-derived fluids prior to eruption of the SUM (Smith, 2010; Marshall et al., 2017b). However, some NVF xenoliths have serpentine filling fractures in olivine and pyroxene. The source of the fracture filling serpentinizing fluid is unknown but may be syn- or post-emplacement, and so would not be representative of the SCLM. This fracture-filling serpentine (FFS) is texturally distinct from serpentine formed at depth (Supplementary Fig. S1). FFS is the dominant hydrous phase mainly in samples with little to no early-forming hydrous minerals (e.g., amphibole, chlorite, antigorite). In most modally hydrated samples, FFS is in much lower abundance than the early forming hydrous minerals. For more detailed sample description and petrology, see Behr and Smith (2016) and Marshall et al. (2017a).

In addition to modal metasomatism, Marshall et al. (2017b) found high δD values (-79 to -33%) relative to the average mantle ($\sim\!-80\%$) in early forming hydrous minerals in these xenoliths and a correlation between increasing indices of metasomatism (Ce/Sm in clinopyroxene) and decreasing olivine $\delta^{18}O$ values in NVF xenoliths. These data indicate that SCLM beneath the Colorado Plateau had been metasomatized by a low- $\delta^{18}O$ fluid/melt from the subducted Farallon slab. NVF xenoliths have also been previously analyzed for major and trace elements, water content, and radiogenic isotope ratios (Behr and Smith, 2016; Bernard et al., 2019; Bizimis et al., 2007; Marshall et al., 2018; Marshall et al., 2017a; Marshall et al., 2017b; Smith, 1979, 2000, 2010, 2013; Smith and Levy, 1976; West et al., 2004), but no halogen data have previously been reported.

2.1.2. Anhydrous North American Peridotite Xenoliths

In addition to the modally hydrated xenoliths from the Navajo Volcanic Field, anhydrous North American SCLM xenoliths from Cerro Chato, Elephant Butte, Kilbourne Hole, and San Carlos were analyzed. Eleven xenoliths from Cerro Chato were analyzed in this study. Cerro Chato is a <700 ka cinder cone in the Zuni-Banderas Volcanic Field on the eastern margin of the Colorado Plateau

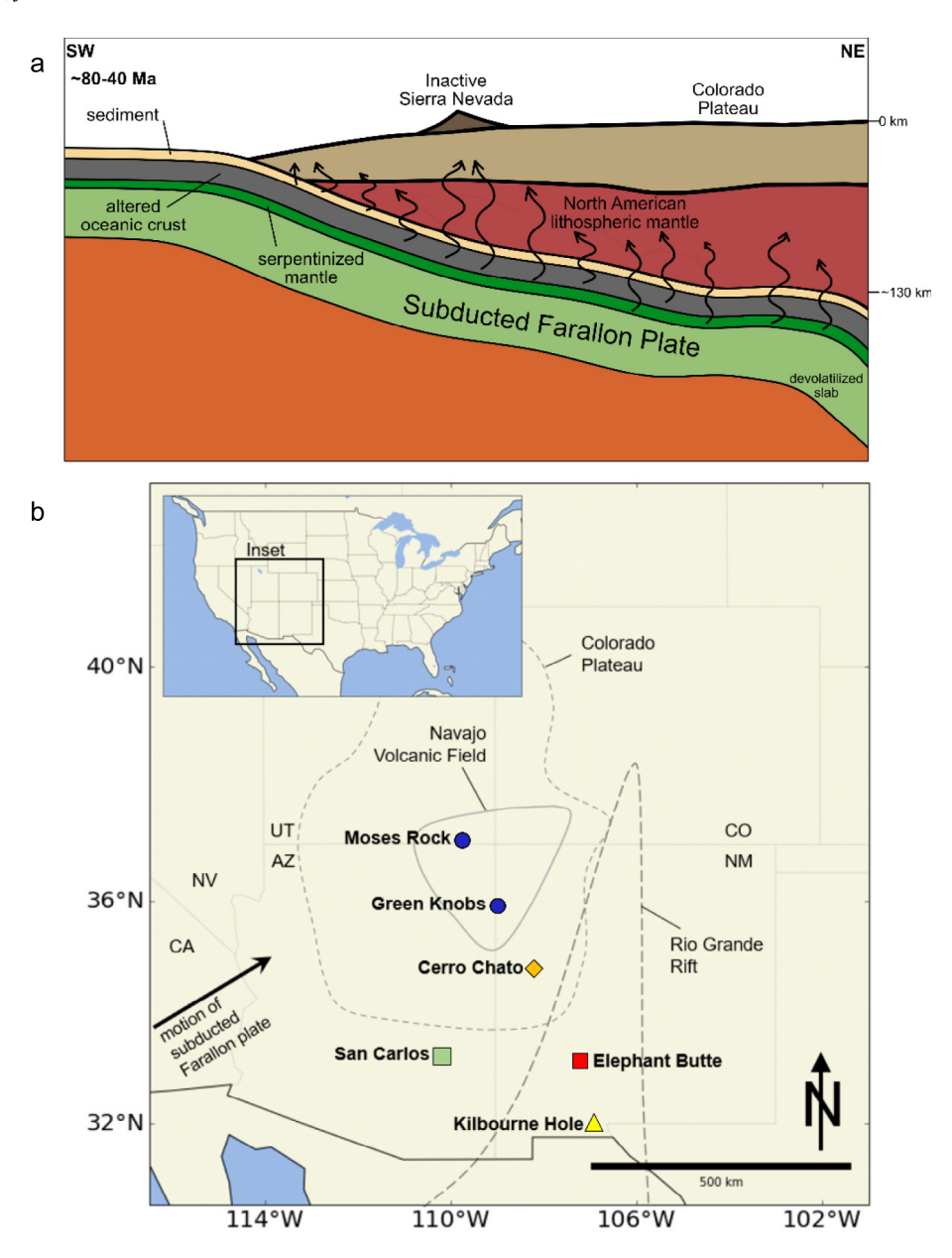


Fig. 1. (a) Cross section of North American lithosphere and the subducting Farallon Plate based on Humphreys et al. (2003). Various subducted lithologies (sediments, altered oceanic crust, serpentinized oceanic mantle) dehydrate when hydrous phases become unstable, releasing hydrous fluids containing variable quantities of halogens. Since the Farallon Plate is in contact with the North American SCLM, fluids rising from the dehydrating slab metasomatize the overlying SCLM. (b) Map of the SW United State from which the North American SCLM samples were collected.

(Fig. 1b) (Laughlin et al., 1993). Xenoliths are all trachybasalthosted spinel lherzolites that have been interpreted as Proterozoic SCLM originating from depths of 55–65 km (Byerly and Lassiter, 2012). These xenoliths have been previously analyzed for major and trace elements and radiogenic isotopes by Byerly and Lassiter (2012, 2015). All xenoliths are spinel peridotites that are divided into two groups following Frey and Prinz (1978). Group-I xenoliths are olivine-rich lherzolites, harzburgites, and dunites. Group-II are cpx-rich lherzolites. Only one Cerro Chato xenolith (CC07-1-23) in this study is from Group-II. Samples have been examined petrographically and no signs of surficial contamination have been found. For more detailed sample descriptions and petrology, see Byerly and Lassiter (2012). Although anhydrous, these xenoliths display variable degrees of metasomatic enrichment (e.g., LREE enrichment) (Byerly and Lassiter, 2012).

Mantle xenolith suites from Elephant Butte (n = 11) and Kilbourne Hole (n = 2) along the southern Rio Grande Rift were also analyzed for bulk halogen content. The Rio Grande Rift formed after the end of the Laramide Orogeny, likely associated with a shift from a compressional to extensional stress regime (Humphreys, 1995; Lawton and McMillan, 1999). The rift stretches from central Colorado to northern Mexico (Fig. 1b). Rifting and associated volcanism began \sim 36 Ma in the south and \sim 27 Ma in the north (Chapin, 1979; Mack et al., 1994). After early volcanism associated with rifting, there was a period of volcanic quiescence in the Miocene followed by a shift in the composition of erupted lavas after 10 Ma towards more depleted Sr and Nd isotopic compositions and more variable Pb isotopic compositions (Baldridge et al., 1980; McMillan et al., 2000). This shift is likely associated with a shift from lithospheric to asthenospheric mantle melting after

removal of the lower SCLM beneath the southern Rio Grande Rift and replacement with asthenosphere (McMillan et al., 2000; Byerly and Lassiter, 2012). The SCLM beneath the southern Rio Grande Rift also experienced some degree of metasomatism from fluid/melt from the subducted Farallon plate (Rowe and Lassiter, 2009; Harvey et al., 2012; Rowe et al., 2015; Urann et al., 2017).

Elephant Butte consists of cinder cones and lava flows that formed during or after the Pliocene (Bachman and Mehnert, 1978; Baldridge, 1979). Mantle xenoliths are mostly basalt- and trachybasalt-hosted spinel lherzolites. Peridotite xenoliths at Elephant Butte are divided into Group-I and Group-II after Frey and Prinz (1978). However, only Group-I peridotites were examined in this study. Small amounts (<1%) of interstitial glass are present along grain boundaries in some samples, as was also observed by Byerly and Lassiter (2015), but no other grain boundary phases were observed. Signs of surficial alteration were present in two xenoliths (BELB 4-30 and BELB 5-8) but in no others.

Elephant Butte samples are divided into refractory and fertile xenoliths. Byerly and Lassiter (2012) interpreted refractory xenoliths as Proterozoic SCLM based on their high spinel Cr#, low Al₂O₃, low clinopyroxene (cpx) modal abundance, and rare earth element (REE) patterns and radiogenic isotope values similar to those of Colorado Plateau SCLM. Byerly and Lassiter (2012) also interpreted fertile xenoliths as recently emplaced asthenosphere based on their high spinel Cr#, high Yb content in cpx, Al₂O₃ contents similar to the depleted mantle, Os isotope compositions similar to abyssal peridotites, and Sr and Nd isotope compositions distinct from Colorado Plateau xenoliths but overlapping and extending the depleted MORB Sr-Nd field. Although Elephant Butte xenoliths do not have evidence of modal metasomatism, there is evidence for metasomatism of the southern Rio Grande Rift mantle from elevated Cl/K and Cl/Nb in olivine-hosted melt inclusions (Rowe and Lassiter, 2009; Rowe et al., 2015).

Kilbourne Hole is an 80 ka volcanic maar that is part of the Potrillo Volcanic Field on the axis of the Rio Grande Rift (Bussod and Williams, 1991, Thompson et al., 2005). Kilbourne Hole xenoliths are spinel lherzolites hosted in basanatic lavas (Bussod and Williams, 1991). Previous studies indicate that Kilbourne Hole mantle xenoliths have been metasomatized by melt-rock reaction (Harvey et al., 2012) or by interaction with a melt/fluid from dehydrating altered oceanic crust in the subducted Farallon plate (Perkins et al., 2006; Urann et al., 2017).

One peridotite xenolith from the San Carlos Volcanic Field in the Basin and Range Province was analyzed for bulk halogen content (Fig. 1b). San Carlos is a late Tertiary to Quaternary volcanic field composed of basaltic cinder cones and basalt flows that host peridotite xenoliths. The one San Carlos xenolith in this study (SC-23) is an equigranular spinel lherzolite that is type-I according to the classification scheme of Frey and Prinz (1978).

Taken together, the xenolith samples from Cerro Chato, Elephant Butte, Kilbourn Hole, and San Carlos represent mantle that has experienced varying degrees of Farallon-slab-related cryptic metasomatism but that lack the modal metasomatism observed in the NVF samples.

2.2. Other Xenoliths: Oahu and Eifel

In addition to North American peridotite xenolith, we analyzed peridotite xenoliths from Oahu, Hawaii and the West Eifel Volcanic Field. These xenoliths are used as a comparison with oceanic lithospheric mantle and other metasomatized SCLM, respectively. We analyzed spinel lherzolite xenoliths (n = 7) from the Salt Lake Crater vent and Pali-Kaau vents on Oahu. These samples are extremely fresh with no evidence for modal metasomatism or serpentinization (Bizimis et al., 2007). These xenoliths are hosted in the alkalic rejuvenation stage of Koolau volcano (Clague and Frey, 1982;

Bizimis et al., 2007). The Pali-Kaau xenoliths are LREE-depleted and Mg- and Cr-rich, indicating that they are residues of the Pacific mantle lithosphere (Bizimis et al., 2007). Salt Lake Crater xenoliths have been interpreted as recycled lithospheric mantle based on their extremely depleted Os and Hf isotope compositions (Bizimis et al., 2007). However, recent work has shown that ultra-depleted domains are more ubiquitous in the DMM than previously thought (Stracke et al., 2011; Byerly and Lassiter, 2014; Lassiter et al., 2014). Therefore, Salt Lake Crater xenoliths may represent ultra-depleted Pacific mantle lithosphere (Chatterjee and Lassiter, 2016).

We analyzed one alkali basalt-hosted spinel lherzolite xenolith from the Quaternary West Eifel Volcanic Field. The European SCLM beneath the Eifel Volcanic Field has a complex history of metasomatism and refertilization. Sr-Nd-Pb isotopes and trace elements suggest three stages of metasomatism from fluids derived from an EM-like component and melts derived from HIMU-like and mixed EM-HIMU sources (Wedepohl et al., 1994; Witt-Eickschen et al., 2003; Bekaert et al., 2019). Metasomatism has been proposed to result either from interaction of the SCLM with mantle plumes or dehydration of an ancient subducting slab (Wedepohl et al., 1994; Rizzo et al., 2021).

3. Experimental methods

3.1. Sample preparation and modal abundance estimates

Interior portions of each xenolith, devoid of any visible weathering or reaction rinds from interaction with the host lava, were selected for analysis and cleaned through ultrasonication in 18.2 $M\Omega$ water and dried on a hot plate. The samples were coarsely crushed with a steel mortar and pestle and powdered with an alumina ceramic ball mill. The powders were rinsed 5 times with 18.2 $M\Omega$ water to remove any potential preparation and storage contamination. The samples were then dried in an oven for two days at $\sim\!40$ °C. Rinsing powders with 18.2 $M\Omega$ water results in loss of halogens in water-soluble phases such as fluid inclusions. It is possible that fluid inclusions can be retained in the powders if the inclusions are smaller than the grain size of the powder (e.g. Urann et al., 2020). However, it is more likely that fluid inclusions present in the samples were lost during the cleaning process, and halogens extracted via pyrohydrolysis are structurally bound.

Modal abundances of hydrous minerals were determined for a subset of samples via point counting on a thin section using a petrographic microscope, point counting on BSE and EDS element maps acquired using a JEOL JSM 6490LV Scanning Electron microscope at UT Austin, and using a Rietveld refinement method on XRD spectra collected using a Bruker D8 Advance X-Ray Diffractometer at UT-Austin. Hydrous mineral abundances are included in the supplementary materials.

3.2. Pyrohydrolysis

Halogens were extracted from the samples via pyrohydrolysis (Schnetger and Muramatsu, 1996; Shimizu et al., 2015). Approximately 1 g of dried sample powder was mixed with \sim 1 g of 99.99% pure vanadium pentoxide flux and added to a cleaned quartz tube. Quartz wool was placed at both ends of the quartz tube to prevent sample loss, before 18.2 M Ω water vapor was passed over the sample as the sample was fused using a gasoxygen flame, releasing the volatile halogens. The halogens were then entrained in the water vapor stream and condensed with a water-cooled condenser. The condensed fluid then directly entered a 20 mM NaOH solution in a clean Pyrex beaker to prevent the volatilization of Br and I. After the complete fusion of the sample,

the interior of the apparatus was rinsed into the Pyrex beaker to ensure that all halogens released from the fused sample were collected. The solutions were then added to clean Nalgene bottles and weighed.

3.3. Fluorine and chlorine

The Cl and F contents of the pyrohydrolysis solutions were determined using a Dionex ICS 2000 Ion Chromatograph. 25 μL of each solution was injected into the ion chromatograph. Calibration standards with 0.1, 0.5, 1, 2.5, and 10 ppm F and Cl in solution were used. Any solution with a F or Cl concentration lower than 0.1 ppm was reanalyzed by injecting 125 μL of solution into the ion chromatograph and running calibration standards with 5, 10, 25, 50, 100, 200, and 500 ppb F and Cl in solution. Detection limits for both F and Cl are 5 ng/g in solution. The bulk xenolith halogen contents were calculated from the mass of powder fused, the volume of pyrohydrolysis solution, and the F and Cl concentration of the solution.

Blanks from the fusion of vanadium pentoxide flux were analyzed to determine the F and Cl content introduced by the flux. Multiple batches of flux were used, and 1–4 splits of each batch were analyzed. The F and Cl contents of the xenoliths were then corrected for contribution from the flux using the blank determined from the specific flux batch used for each sample. The F and Cl content of different splits of each batch of flux were homogenous, with a contribution of Cl and F of <1–70% (average <20%) and <27% of the total concentration of the samples, respectively. All reported F and Cl xenolith concentrations are flux-corrected (details of flux halogen contents and blank corrections are in supplementary materials). Any sample for which the flux correction is >50% of the total sample is reported as less than the maximum possible concentration (see supplementary material).

The halogen yields from pyrohydrolysis were determined by fusing reference materials BHVO-2 and BCR-2. Using GeoReM preferred values (Jochum et al., 2015), the average F yields are $102 \pm 3\%$ for BCR-2 and $101 \pm 3\%$ for BHVO-2, and the average Cl yields are $82 \pm 6\%$ for BCR-2 and $78 \pm 12\%$ for BHVO-2 (Supplementary Table S2).

3.4. Bromine and Iodine

Br and I concentrations of the mantle xenoliths were determined using a Thermo Element2 at the University of Texas at Austin (UT Austin) and Br concentrations were also determined using a Thermo Scientific Element XR at the Freie Universität in Berlin (FU Berlin) using high-resolution inductively coupled plasma mass spectrometry (HR-ICP-MS). Methods for sample preparation and halogen detection at UT Austin and FU Berlin differ slightly but were both modified from Bu et al. (2003). At UT Austin and FU Berlin, 5.4 g of sample pyrohydrolysis solution was mixed with 0.6 g of 100 μg/L Te (UT Austin) or In (FU Berlin) solution to correct for drift in signal intensities over time. Calibrations standards with 0.5, 1, 2, 3, and 5 μ g/L and 0.25, 1.25, 2, 6, 15, and 60 μ g/L Br and I were used at UT Austin and FU Berlin, respectively. At UT Austin, calibration standards and blanks were ~2 mM NaOH to approximate the NaOH molarity of the sample solution and thus reduce any effect of the matrix on the ionization of Br and I. After two washes of 2 mM NaOH, a sample was analyzed, followed by two washes of 5% ammonia hydroxide to remove any excess Br and I. This process was repeated for every sample and reference material. The background Br and I were measured on the second 2 mM NaOH wash prior to sample analysis, and this value was used to correct the Br and I content of the subsequent sample. The Br and I backgrounds were stable throughout the course of each analytical session, and background corrections yield reproducible results when

re-analyzing aliquots of the same solution (1σ = \sim 6 ppb Br and \sim 16 ppb I in the rock). The method at FU Berlin was similar, but calibration standards and blanks were prepared in 50 mM NaOH instead of 2 mM NaOH. Br contents of the same pyrohydrolysis solutions from 12 samples were measured at UT Austin and FU Berlin to cross-calibrate the labs and fall on a 1:1 line (Fig. S2). Method detection limits varied throughout the analytical sessions but ranged from 0.06 to 0.5 ppb Br in solution and 0.09–0.15 ppb I in solution, which correspond to \sim 6–75 ppb Br and \sim 5–22 ppb I in the rock before blank correction.

Procedural blanks from the fusion of vanadium pentoxide flux were analyzed to determine the Br and I content introduced by the flux. The Br and I content of different flux batches varied dramatically from 8 to 680 ppb Br and 4 to 530 ppb I, and I was generally in higher abundance in the flux (see Fig. S3). Heating of flux to 600 °C for 3-16 h to remove volatiles resulted in dramatic lowering of halogen content of the flux (8-16 ppb Br and 4-25 ppb I) compared to the same flux batch prior to heating (165-680 ppb Br and 90-103 ppb I) (see supplementary material for more details). Samples fused with fluxes that have high and heterogeneous Br and I contents are not reported nor considered in the interpretation of these samples (see supplementary materials for more details). In the remaining samples, flux-derived Br and I contribute an average of 21% and 28% of the total concentration of the samples, respectively. All reported Br and I xenolith concentrations are fluxcorrected. Any sample for which the flux correction is >50% is reported as less than the maximum possible concentration (see supplementary material).

Br and I yields from pyrohydrolysis were determined by fusing reference materials BCR-2 and BHVO-2. Using GeoReM preferred values for BCR-2 and BHVO-2, Br yields average 101 ± 40% and 99 ± 49%, respectively after flux correction, and are within the range of reported uncertainty. Iodine yields for BCR-2 and BHVO-2 after flux correction average 97 \pm 88% and 317% of the GeoReM preferred values, respectively (Supplementary Table S2). Although the measured BCR-2 I contents are within the acceptable range of GeoReM preferred values, the measured BHVO-2 I content are significantly higher. Only one BHVO-2 sample was melted without significant I contamination from the flux. This BHVO-2 split was fused without flux on the same day as the flux blank with the lowest I content (4 ng/g), and so additional contamination introduced during the pyrohydrolysis procedure is unlikely. This BHVO-2 reference material has an I content (63 ppb I) higher than the GeoReM preferred value (20 ppb I). However, this value falls within the range of I contents for BHVO-2 from other studies (range= <16 ng/g to > 300 ng/g: Sekimoto and Ebihara, 2016; Michel and Villemant, 2003), and is consistent with the study of Kendrick et al (2018) which reports 70 + / - 4 ppb I for BHVO-2. Therefore, we consider this I content to reflect yields similar to those of previous studies. Due to inconsistency in the I concentrations of BHVO-2 in the literature and the disagreement between I contents of BHVO-2 in this study, BHVO-2 does not appear to be an appropriate reference material for I.

Replicate analyses (representing sample preparation, fusion, and analysis) were performed on a subset of samples for F (n = 20), Cl (n = 24), Br (n = 7), and I (n = 6) and indicate a 2σ sample reproducibility of 2.2 ppm F, 9.0 ppm Cl, 22.6 ppb Br, and 81 ppb I (Supplementary Fig. S4). However, sample reproducibility is not consistent across all concentrations for Cl, Br, and I. Relative standard deviation (RSD) (1σ) in these halogen concentrations decreases from \sim 30% at 1 ppm Cl to \sim 6% at 100 ppm Cl and from \sim 100% at 2 ppb Br to \sim 5–15% at 100–300 ppb Br. RSD for I are higher and more variable and ranges from 10% to >100%. Standard deviations from replicate analyses are reported for samples for which multiple aliquots of powder were fused and analyzed, For samples for which only one aliquot was fused and analyzed,

representative external errors at the given halogen content of that sample are reported (see supplementary materials).

Multiple analyses of I in a single solution are far more consistent than sample replicates, I backgrounds are consistently <0.1 ppb in solution, and calibration standards as low as 0.15 ppb have successfully been analyzed. All of these indicate that an external factor is affecting the reproducibility of I analyses. Unobserved heterogeneity in the blank or in the samples themselves could explain some of the variability. I data are reported but many have large errors (RSD > 50%).

3.5. Oxygen isotopes

Olivine $\delta^{18}O$ ($\delta^{18}O_{olv}$) values were measured using the laser fluorination method of Sharp (1990) at UT Austin using a ThermoElectron MAT 253 mass spectrometer. Approximately 2 mg of optically clear olivine were hand-picked under a binocular microscope to ensure sample homogeneity. Garnet standard UWG-2 ($\delta^{18}O$ = +5.8%; Valley et al., 1995), in-house olivine standard San Carlos ($\delta^{18}O$ = +5.3%), and in-house quartz standard Lausanne-1 ($\delta^{18}O$ = +18.1%) were analyzed to determine accuracy and precision. All $\delta^{18}O$ values are reported relative to VSMOW. Error on replicates of in-run standards is < 0.07% (1SD) and on sample duplicates is < 0.05% (1 SD).

4. Results

4.1. Fluorine and chlorine concentrations

The F and Cl contents of all suites of anhydrous xenoliths from Elephant Butte, Cerro Chato, Kilbourne Hole, San Carlos, Hawaii, and Eifel range from 1 to 41 ppm (average = 17 ppm) and 1–17 ppm (average = 5 ppm), respectively (Table 1). While these values extend higher than DMM F (12–16 ppm) and Cl (0.5–10 ppm) estimates, the averages are similar to DMM concentrations (Schilling et al., 1980; Burgess et al., 2002; Saal et al., 2002; Simons et al., 2002; Salters and Stracke, 2004; Shaw et al., 2010; Kendrick et al., 2012; Le Voyer et al., 2015; Shimizu et al., 2016; Kendrick et al., 2017; Urann et al., 2017). These F and Cl ranges are also similar to those observed by Kobayashi et al. (2019) and Beyer et al. (2012) in anhydrous lithospheric mantle xenoliths from Eifel; Kilbourne Hole; San Carlos; Hualalai; Lanzarote, Canary Islands; and Mt. Leura, Australia (Figs. 2a, 3a, 3c), but extend to slightly higher Cl contents.

Using previously reported whole-rock trace element abundances from Byerly and Lassiter (2012) and Marshall et al., (2017a, 2017b), the F/Nd of the anhydrous xenoliths range from 4 to 60 with an average ratio of 20, similar to the canonical DMM F/Nd=~21 ± 5 (Workman et al., 2006) with the exception of the refractory Elephant Butte xenoliths and one fertile Elephant Butte xenolith that have F/Nd = 80–700 (Fig. 3a). Cl/Nb of anhydrous xenoliths range from 5 to 65 (Fig. 3b) with an average ratio of 18.3, similar to Cl/Nb in pristine MORB glasses (average = 21) (Kendrick et al., 2017), but higher than Cl/Nb from previous anhydrous SCLM xenolith analyses of Kobayashi et al. (2019) which generally fall below DMM values.

Modally hydrated xenoliths from the Navajo Volcanic Field have F and Cl concentrations that range from <2–47 ppm and 31–574 ppm, respectively (Table 1). F contents span a similar range as those of the anhydrous xenoliths from this study and are generally comparable to the F content of DMM (Fig. 3a). However, F/Nd values (2–1297; median = 52) are higher than DMM (\sim 21; Workman et al., 2006) and previously reported SCLM ratios (Urann et al., 2017). The Cl concentrations (30–570 ppm) of the NVF xenoliths are significantly higher than for estimates of the

DMM and the anhydrous xenoliths from this study. Cl/Nb in the NVF xenoliths range from \sim 100–17,800, significantly higher than those of MORB, but similar to Cl/Nb of arc basalts (43–7128) (Saal et al., 2002; Salters and Stracke, 2004; Workman et al., 2006; Kendrick et al., 2017; Kendrick et al., 2020).

Cl contents of the modally hydrated xenolith suite do not correlate with extent of modal hydration or LOI (Fig. 4 and S5), and Cl does not correlate with indices of metasomatism such as Ba/Nb in the whole rock or clinopyroxene separates for any xenolith suite. F contents of the NVF xenoliths do correlate with LOI and modal hydration (Figs. 4 and S5). There is a positive correlation between xenolith Cl/Nb and whole rock Ba/Nb in NVF xenoliths and when all xenolith suites are combined. This general correlation is defined by two endmembers: NVF xenoliths with high Cl and Ba, and the anhydrous xenoliths with low Cl and Ba (Fig. 5b).

4.2. Bromine and Iodine concentrations

Flux-corrected Br and I content of Oahu samples were only collected for Salt Lake Crater samples, and are 45-53 ppb and 270 ppb, respectively. Bromine and I concentrations are systematically elevated relative to estimates for DMM. However, due to the large external error on I measurements, I concentrations in most anhydrous xenoliths are within 2 standard deviations of DMM (~0.3 ppb I; Kendrick et al., 2017). Additionally, Br/Cl is elevated (0.008-0.04) relative to MORB/OIB (~ 0.003 ; Kendrick et al., 2017), though within 1 standard deviation of the upper range of MORB/OIB (Fig. 2). While Salt Lake Crater samples with Br data do not have Nb concentrations on the exact same samples, previous analyses of the Salt Lake Crater xenoliths show a limited range of Nb contents of 0.47-1.54 ppm (Chatterjee and Lassiter, 2016). Using an average of these values, the Br/Nb falls within the range of MORB/OIB (Fig. 3c). The Nb contents of these xenoliths are ~2-7 times higher than estimated DMM Nb contents (Salters and Stracke, 2004).

Flux-corrected Br and I content for all suites of variably, cryptically metasomatized anhydrous SCLM xenoliths from Elephant Butte, Cerro Chato, Kilbourne Hole, San Carlos, and Eifel range from <7–190 ppb and 30–260 ppb, respectively (Table 1).

Modally hydrated NVF xenoliths have Br and I concentrations of 79–880 ppb and <7–265 ppb, respectively, similar to the range of I contents in the anhydrous xenoliths. These Br concentrations overlap with the anhydrous xenolith Br range but extending to higher concentrations. Br and I concentrations for all xenoliths in this study range from DMM-like to 1,000 times greater than the estimated DMM concentrations (13 ppb Br and 0.3 ppb I; Kendrick et al., 2017; Fig. 2b-d). Furthermore, the Br and I content of these xenoliths are higher than the range previously reported for other lithospheric mantle xenoliths from Eifel, San Carlos, and Kilbourne Hole (0.6-9 ppb Br and 0.1-0.8 ppb I; Kobayashi et al., 2019). The Br and I content of the analyzed xenoliths are similar to the range found in subduction-influenced intraplate xenoliths from the West Antarctic Rift System and Udachnaya, Siberia (Broadley et al., 2016, 2018) and mantle wedge xenoliths (Kobayashi et al., 2017) (Fig. 2b-c).

Neither the Br nor I content within any single analyzed xenolith suite correlates with modal hydration or LOI (Figs. 4 and S5). However, the Br/Nb in NVF xenoliths and combined Br/Nb and I/Nb for all xenolith suites broadly correlates with whole rock Ba/Nb (Fig. 5c,d). Additionally, Br and Cl are positively correlated in the NVF xenoliths, but not in any other xenolith suite (Fig. 2b).

4.3. Filtering for late-stage alteration

Several xenoliths from the Navajo Volcanic Field have variable amounts (\sim 0 to 18 modal %) of fracture-filling serpentine (FFS) that

Table 1 Whole rock halogen abundance in xenoliths.

Sample Name	Locality	Xenolith source	Metasom.	Modal % Hydrous Minerals	% FFS	F (ppm)	±	Cl (ppm)	±	Br (ppb)	±	I (ppb)	±
Anhydrous peridotite													
07EB1.01	EB	AM	Cryptic	0	_	32	1.3	3	1.6	98	49		
07EB1.05	EB	AM	Cryptic	0	-	28	1.8	10	1.4	190	19		
07EB2.03	EB	AM	Cryptic	0	_	10	1.1	<6		86	21		
07EB4.01	EB	AM	Cryptic	0	_	18	10.2	<4		70	33		
07EB4.05	EB	AM	Cryptic	0	_	15	1.1	<3				258	114
BELB9-6	EB	AM	Cryptic	0	_	30	0.6	12	0.8	86	9	38	4
BELB9-8	EB	AM	Cryptic	0	_	31	0.5	16	2.3	92	37		
07EB1.11	EB	SCLM	Cryptic	0	_	41	1.1	2				102	53
BELB9-15	EB	SCLM	Cryptic	0	_	40	0.7	17	1.9	95	15		00
CC07-1-14	CC	SCLM	Cryptic	0	_	8	0.8	5	3.7	126	27		
				0	_	1		6	1.5	181			
CC07-1-04	CC	SCLM	Cryptic				0.1		1.5		32		
CC07-1-06	CC	SCLM	Cryptic	0	_	11	1.1	<3	2.0	93	32		
CC07-1-20	CC	SCLM	Cryptic	0	_	8	0.5	8	3.9	64	8		
CC07-1-22	CC	SCLM	Cryptic	0	_	7	1.1	3	1.1	134	13		
CC07-1-23	CC	SCLM	Cryptic	0	_	24	1.1	5	1.2	86	17		
CC07-1-26	CC	SCLM	Cryptic	0	_	11	0.7	<2		73	21		
CC07-1-35	CC	SCLM	Cryptic	0	_	8	2.2	<3		51	8	30	25
CC07-1-51	CC	SCLM	Cryptic	0	_	19	1.1	<6		104	25		
CC07-2-01	CC	SCLM	Cryptic	0	_	26	1.1	10	1.4	-	-		
CC07-3-01	CC	SCLM	Cryptic	0	_	10	0.6	3	0.8	90†	120		
10KH27	KH	SCLM		0	_	7	2.6	4	0.8	82	21		
			Cryptic	0								72	42
KH2	KH	SCLM	Cryptic		_	11	2.2	1	0.6	75	12	72	42
SC23	SC	SCLM	None	0	_	4	0.9	1	0.5	<7		36	28
DW8	EVF	SCLM	Cryptic	0	_	8	0.7	3	1.3	46	18	81	45
NMNH 114745-3	OH-P	OLM	None	0	_	23	1.1	2	1.0				
NMNH 115048-2	OH-SLC	OLM	MI	0	_	14	1.1	3	1.1				
NMNH 115048-26	OH-SLC	OLM	MI	0	_	18	1.1	5	1.1				
KAPS-36	OH-P	OLM	None	0	_	9	1.1	<3					
SLC 319	OH-SLC	OLM	MI	0	_	28	1.1	5	1.2				
SLC 405	OH-SLC	OLM	MI	0	_	9	0.6	1	0.1	45†	87		
SLC 470	OH-SLC	OLM	MI	0	_	8	0.8	6	0.3	53	21	270	15
Modally hydrated pe		OLIVI	IVII	U		0	0.0	U	0.5	33	21	270	13
		SCLM	Modal	55.1 ²	<5	6	11	160	7.8	229	10		
EMGN10	NVF-GN						1.1	160			18		
EMGN12	NVF-GN	SCLM	Modal	28.7 ²	10	<5		142	7.0	308	16		
EMGN14	NVF-GN	SCLM	Modal	46 ²	_	23	1.1	182	8.7	382	35		
EMGN17	NVF-GN	SCLM	Modal	30.6 ²	15	26	1.1	266	12.3				
EMGN2	NVF-GN	SCLM	Modal	<5 ²	>95	6	1.1	79	4.3				
EMGN21	NVF-GN	SCLM	Modal	32.4 ²	20	20	1.1	156	7.6				
EMGN23	NVF-GN	SCLM	Modal	13.8 ³	_	3	1.1	210	10.0				
EMGN24	NVF-GN	SCLM	Modal	25.1 ²	<5	26	1.1	58	3.4	130	12		
EMGN26	NVF-GN	SCLM	Modal	20 2	90	15	1.1	148	7.3				
				31 ³	30		1.1			252	11		
EMGN27	NVF-GN	SCLM	Modal			42	1.1	226	10.6	353	41		
EMGN29	NVF-GN	SCLM	Modal	2 2	30	<2		183	8.8	400			
EMGN7	NVF-GN	SCLM	Modal	19.8 2	_	4	1.1	125	6.3	138	19		
EMGN9	NVF-GN	SCLM	Modal	45.5 ³	<5	8	3.2	113	1.6	283	27	<7	
1106-GN	NVF-GN	SCLM	Modal	12.1 ¹	10	3	1.1	263	12.2	163	19		
N126-GN	NVF-GN	SCLM	Modal	4.1 ¹	>95	4	1.1	149	8.4	148	10	<40	
N15-GN	NVF-GN	SCLM	Modal	63.1 ¹	<5	12	1.1	323	14.8	283	18		
N16-GN	NVF-GN	SCLM	Modal	6 ¹	>95	6	1.1	115	5.9		-		
1178-GN	NVF-GN	SCLM	Modal	4.4 ¹	<5	8	1.1	72	4.0	211	17		
1176-GN 117-GN	NVF-GN NVF-GN	SCLM	Modal	6.4 ¹	30	3	1.1	195	9.3	157	11		
												121	
123-GN	NVF-GN	SCLM	Modal	35.2 ¹	<5 	8	1.1	31	3.0	79	30	131	64
N51-GN	NVF-GN	SCLM	Modal	30.4 1	50	6	1.3	286	10.9	270	1	117	55
N55-GN	NVF-GN	SCLM	Modal	5.3 1	15	8	1.1	263	12.2	502	49		
N57-GN	NVF-GN	SCLM	Modal	31.7 ¹	30	3	1.1	178	8.6				
N61-GN	NVF-GN	SCLM	Modal	0.2 1	>95	9	1.1	226	10.6				
N71-GN	NVF-GN	SCLM	Modal	24.3 1	20	14	1.1	269	12.5	331	33		
EMMR4	NVF-MR	SCLM	Modal	79.2 ²	5	47	0.4	211	14.3	331	20	265	72
EMMR7		SCLM	Modal	20.6 ³	_	7		574	25.5	880		203	, 2
	NVF-MR						1.1				71 20		
MR-ATG-13	NVF-MR	SCLM	Modal	18.7 ³	>95	42	1.1	331	15.1	510	26		
Anhydrous peridotite	es with petr	ographic ind	icators of sur	ncial alteration			_	_					
3ELB 4-30						61	2.1	2	1.0	39	17		
BELB 5-8						13	1.1	5	1.1	70	18		

Metasom. = metasomatism type, MI = melt infiltration, Modal = modal hydration. 1-point count data from S. Levy and D. Smith; 2- estimated abundance from petrographic microscope and EDS elemental maps of thin sections; 3- XRD and Rietveld refinement method; %FFS = estimated abundance of fracture filling serpentine (FFS) normalized to the modal % of total hydrous minerals. See Supplementary Material for breakdown of different hydrous phases. †Average includes value includes sample with low yield and are not included in figures. Errors are 1 standard deviation of duplicate analyses. *Italicized error is 1 standard deviation based on variability of external error from sample duplicates*. AM: Asthenospheric mantle, SCLM: Sub-continental lithospheric mantle, OLM: oceanic lithospheric mantle. EB: Elephant Butte, CC: Cerro Chato, NVF-GN: Navajo Volcanic Field- Green Knobs, NVF-MR: Navajo Volcanic Field-Moses Rock, KH: Kilbourne Hole, SC: San Carlos, EVF: Eifel Volcanic Field, OH-P: Pali, Oahu, Hawaii. OH-SLC: Salt Lake Crater, Oahu, Hawaii.

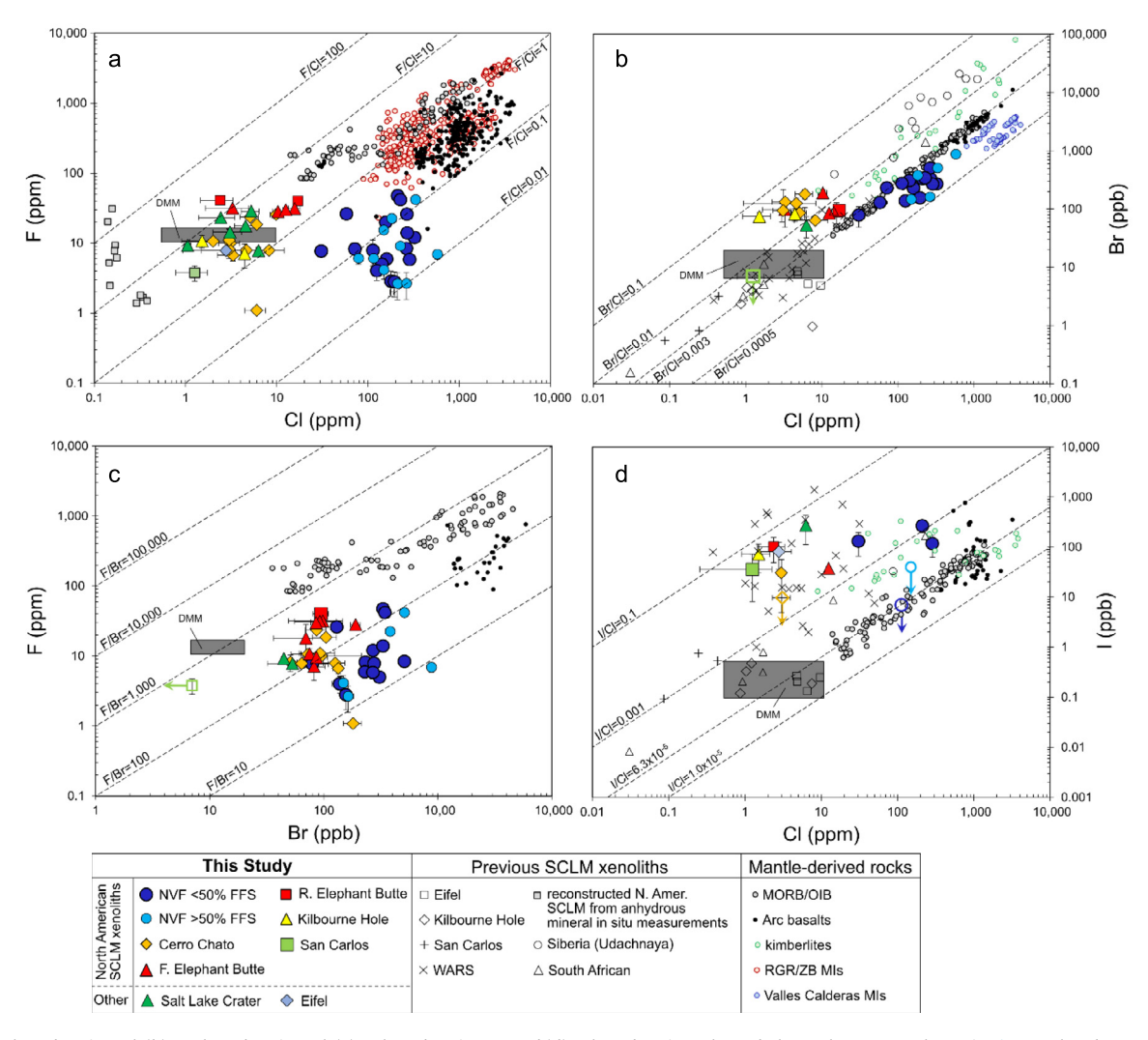


Fig. 2. (a) F plotted against Cl, (b) Br plotted against Cl, (c) F plotted against Br and (d) I plotted against Cl. Symbols are the same as shown in Fig. 1. Colored open symbols with arrows are data with large blank corrections that are reported as less than maximum values. Error bars are 1σ. DMM = Depleted MORB-source Mantle, NVF = Navajo Volcanic Field, FFS = fracture-filling serpentine (see main text), F. Elephant Butte = Fertile Elephant Butte, R. Elephant Butte = Refractory Elephant Butte, S. RGR/ZB MIs = Rio Grande Rift/Zuni-Banderas Volcanic Field melt inclusions, WARS = Western Antarctica Rift System. MORB/OIB data from Kendrick et al. (2017). Arc data from Kendrick et al. (2020) and the compilation from Urann et al. (2017). Published xenolith data from Broadley et al. (2018), Kobayashi et al. (2019), Toyama et al. (2021), and Johnson et al. (2000). Valles Caldera melt inclusion data from Waelkens et al. (2021). Kimberlite data from Toyama et al. (2021). RGR/ZB melt inclusion data from Woee et al. (2015). DMM estimates are based on estimates from Kendrick et al. (2017), Bekaert et al. (2021), Urann et al. (2007), Saal et al. (2006), Shimizu et al. (2016), and Le Voyer et al. (2015).

may result from late-stage, syn- or post-emplacement alteration (Marshall et al., 2018), though the exact source of the serpentinizing fluid is unclear. While nominally anhydrous minerals can retain detectable quantities of halogens (Bernini et al., 2013; Beyer et al., 2012; Dalou et al., 2012; Urann et al., 2017; Urann et al., 2020), late-stage hydrous minerals in mantle xenoliths, particularly serpentine, can contain far higher Cl contents (~100–2,0 00 ppm; Frezzotti and Ferrando, 2018 and references therein). Therefore, FFS likely affect the Cl (and possibly F, Br, and I) content of the xenoliths in which it is the dominant hydrous phase. To avoid major halogen contamination from FFS, any xenolith sample in which the FFS makes up >50% of the hydrous phases in the rock is not considered to have a mantle halogen signature. The proportion of FFS relative to other hydrous minerals in each NVF sample is listed in Table 1.

4.4. Olivine Oxygen isotope ratios

Oxygen isotope ratios in olivine from Cerro Chato, Elephant Butte, and Navajo Volcanic Field xenoliths range from +5.05% to

+5.41‰, and individual analyses are reported in Table 2. These δ^{18} - $O_{\rm olv}$ values are similar to the average mantle olivine $\delta^{18}O$ of 5.14 \pm 0.28‰ (Mattey et al., 1994; Chazot et al., 1997). After filtering for xenoliths in which >50% of the hydrous minerals in the rock are late-stage FFS, there is a negative correlation between [CI], [Br], and Cl/F and $\delta^{18}O_{\rm olv}$ in NVF, Cerro Chato, Elephant Butte, and San Carlos xenoliths (Fig. 6a, c, d). There is no correlation between $\delta^{18}O_{\rm olv}$ and [F] (Fig. 6b).

5. Discussion

5.1. Comparison with previous SCLM

There are differences between the measured bulk xenolith halogen contents of this study and the halogen contents of similar xenoliths from the same localities from previous studies. Cl and F concentrations in the anhydrous xenoliths from Kilbourne Hole, San Carlos, and Eifel reported in this study (1–4 ppm Cl and 4–11 ppm F) are broadly consistent with the Cl range reported in mantle xenoliths from the same localities by Kobayashi et al.

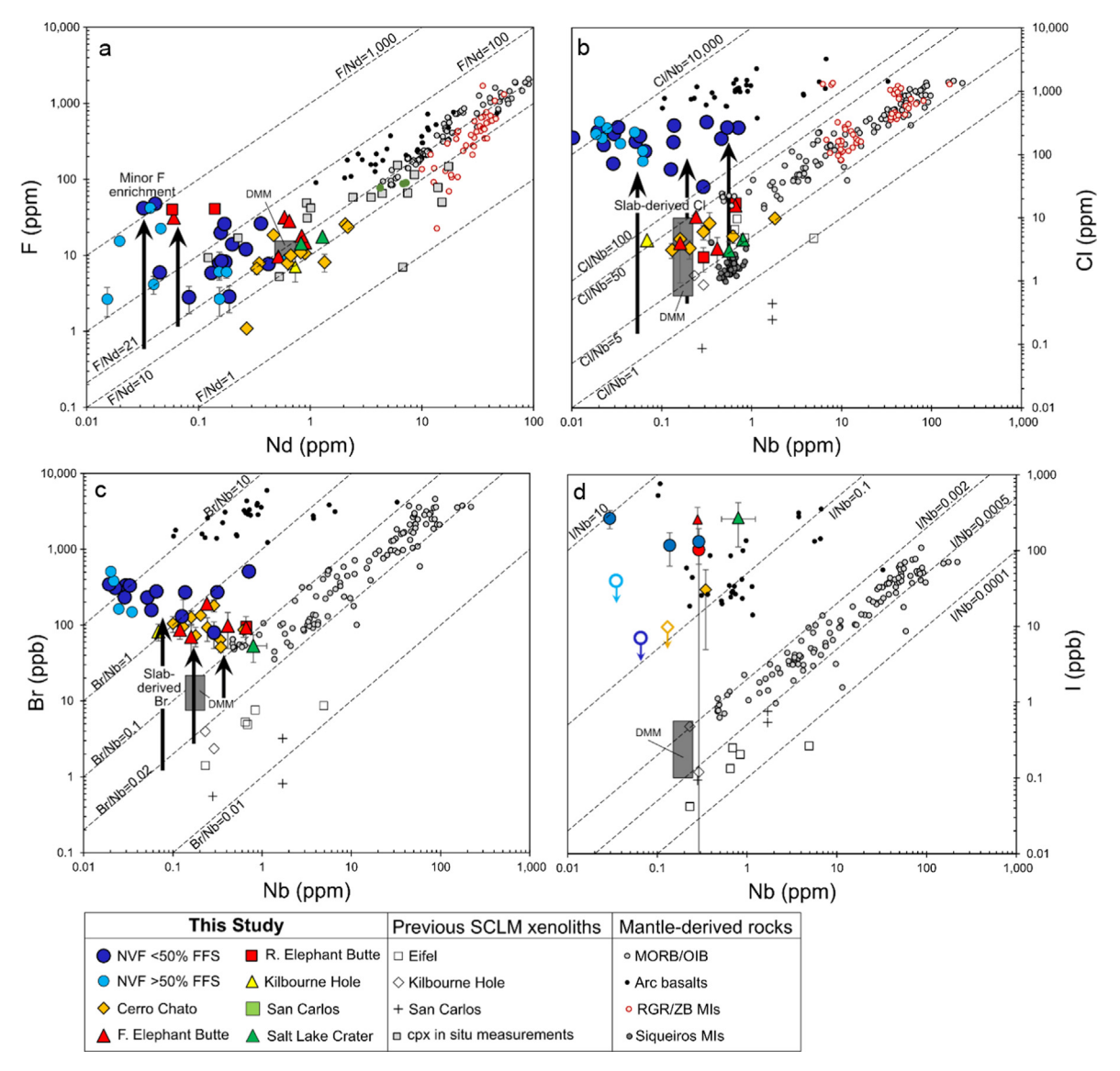


Fig. 3. Halogens plotted against refractory lithophile elements with similar partition coefficients during mantle melting (a) F plotted against Nd and (b) Cl, (c) Br, and (d) I plotted against Nb. Cl, Br, and I are all enriched in the xenoliths from this study relative to MORB and OlB. Colored open symbols with arrows are data with large blank corrections that are reported as less than maximum values. Average Nb content was calculated for Oahu xenoliths with Br data (see text). Error bars are 1σ. DMM = Depleted MORB Mantle, NVF = Navajo Volcanic Field, FFS = fracture-filling serpentine (see main text), F. Elephant Butte = Fertile Elephant Butte, R. Elephant Butte = Refractory Elephant Butte, S. RGR/ZB MIs = Rio Grande Rift/Zuni-Banderas Volcanic Field melt inclusions. MORB/OlB data from Kendrick et al. (2017). Siqueiros MI data from Saal et al. (2002). Arc data from Kendrick et al. (2017) and the compilation from Urann et al. (2017). Previous SCLM xenolith data from Kobayashi et al. (2019) and Gibson et al. (2020). S. RGR/ZB data from Rowe et al. (2015). Trace element data for xenoliths in this study from Marshall et al. (2017a), Byerly and Lassiter (2012), and Chatterjee and Lassiter (2016). DMM estimates are based on estimates from Kendrick et al. (2017), Bekaert et al. (2021), Urann et al. (2017), Saal et al. (2002), Shimizu et al. (2016), Le Voyer et al. (2015), Salters and Stracke (2004), and Workman and Hart (2005).

(2019; 0.1–10 ppm Cl) and the F range reported by Urann et al. (2017; 6–20 ppm F). However, Urann et al. (2017) reported significantly lower Cl contents in SCLM xenoliths from Kilbourne Hole (0.14 ppm Cl) and San Carlos (0.18 ppm Cl). This disagreement likely results from differing measurement techniques. Urann et al. (2017) measured halogen concentrations in olivine, clinopyroxene, and orthopyroxene by SIMS and calculated the bulk xenolith halogen content based upon mineral modal abundances, whereas this study and Kobayashi et al. (2019) measured the halogen content of the bulk xenoliths. The reason for agreement between bulk and *in situ* studies for F but not Cl is likely due to preferential incorporation of F into the lattice of mafic minerals, as observed by Urann et al. (2020). The additional Cl observed in the bulk rock studies may be hosted in phases that were not analyzed by *in situ* mineral analyses, such as along grain boundaries.

Grain boundaries may be an important reservoir for halogens, as has been shown to be the case for incompatible trace elements (Byerly and Lassiter, 2015).

Although [CI] data from San Carlos, Kilbourne Hole, and Eifel are generally within a factor of ~0.5–10 and reproduce with the bulk rock halogen study of Kobayashi et al. (2019), anhydrous xenolith [CI] and CI/Nb from all combined localities are generally elevated relative to SCLM from previous studies and are closer to DMM (Figs. 2 and 3). Additionally, Br and I data in this study from same localities analyzed by Kobayashi et al. (2019) are elevated relative to previous values. The Br and I content of xenoliths from Kilbourne Hole (75–82 ppb Br and 72 ppb I) and Eifel (46 ppb Br and 81 ppb I) from this study are 1–2 orders of magnitude higher than the Br and I contents in xenoliths from those same localities analyzed by Kobayashi et al. (2019; Kilbourne Hole = 1–4 ppb Br,

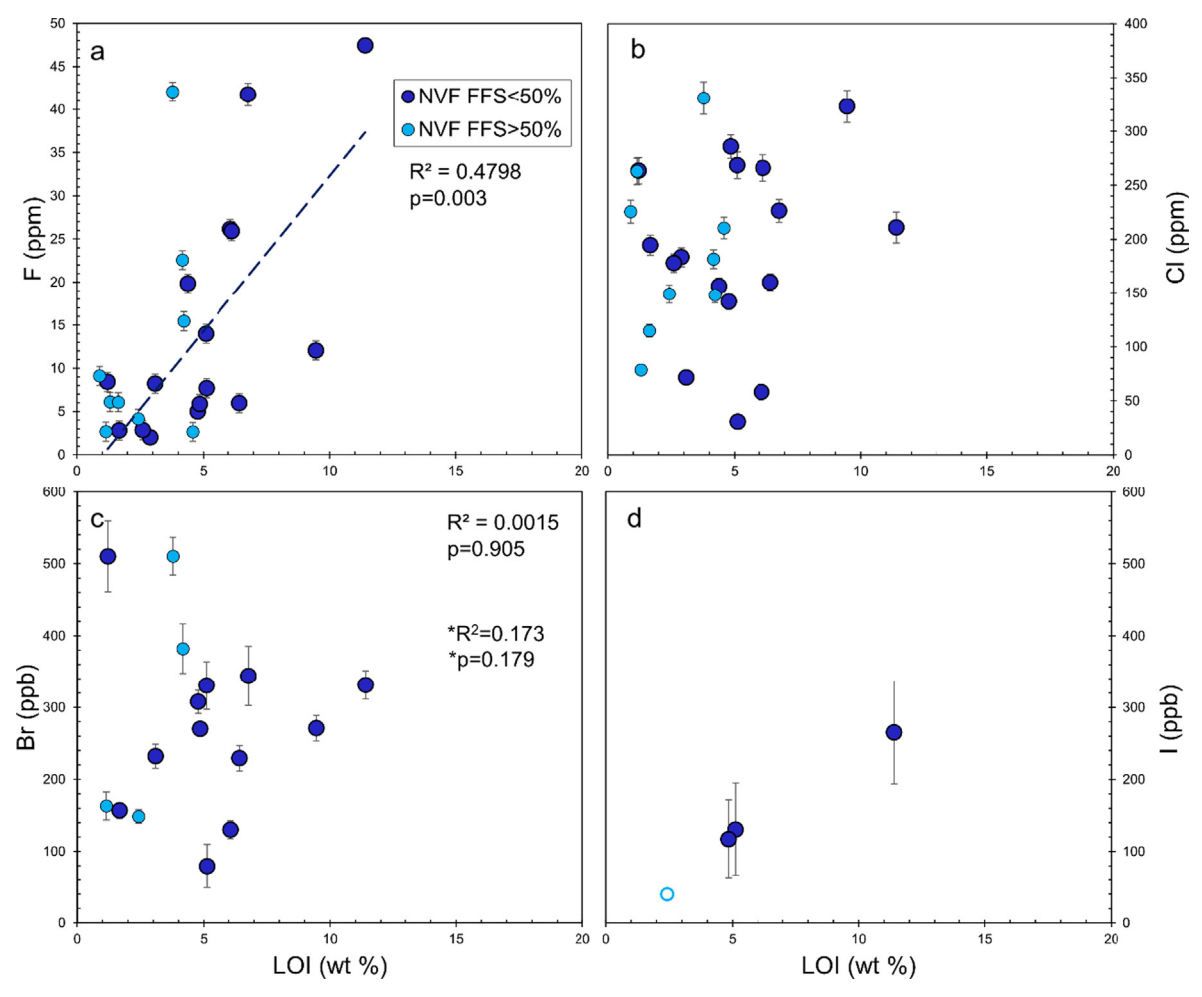


Fig. 4. (a) F, (b) Cl, (c) Br, and (d) I plotted against loss on ignition (LOI). Error bars are 1σ . LOI is a proxy for the total water content in the xenoliths. Some xenolith samples also contain carbonate, reducing the correlation between LOI and water content. However, hydrous minerals compose a much larger fraction of the xenoliths than carbonate, therefore LOI is reasonable proxy for water content. The trend line, R^2 , and p-values (non-directional) are all for a linear regression through the NVF FFS < 50% data. Only F vs. LOI has a p-value < 0.05. * R^2 and *p in (c) describe a linear regression of Br and LOI that does not include the outlier data for N55-GN. LOI data from Marshall et al. (2017a). Colored open symbols are data with large blank corrections that are reported as less than maximum values. NVF = Navajo Volcanic Field. FFS = fracture-filling serpentine.

0.2–0.5 ppb I and Eifel = 1.4–8.6 ppb Br, 0.04–0.3 ppb I). There is a smaller discrepancy between the San Carlos xenolith from this study (<7 ppb Br and 36 ppb I) compared to previously studied San Carlos xenoliths (0.6–3.2 ppb Br and 0.09–0.75 ppb I; Kobayashi et al., 2019). The large error on I measurements may explain the discrepancies for I, but Br concentrations are consistently higher even when considering external error.

The reproducibility of Br and Cl between replicates and between laboratories (for Br; see supplementary material) indicates that the cause of the discrepancy is not analytical, but rather reflects true discrepancy in the halogen contents of the xenoliths. The exact reason for the discrepancies with previous studies is unclear. Surficial alteration of the samples would affect the halogen content of the samples, but all North American samples included in the discussion have been examined petrographically. Only two samples (BELB 4-30 and BELB 5-8) show signs of alteration. These samples are not included in the figures or the interpretations, and so it is unlikely that surficial alteration is the cause of the discrepancy. It is possible that discrepancies in the Br contents, and perhaps the I contents as well, may be indicative of true halogen heterogeneity in xenoliths since different samples were studied.

Alternatively, the differences may result from differing analytical techniques. This study washed samples in 18.2 $M\Omega$ water to remove any water-soluble contaminants, then extracted halogens

from bulk xenoliths through pyrohydrolysis and analyzed them via HR-ICP-MS, whereas Kobayashi et al. (2019) leached their samples in 1 N nitric acid, then used the neutron irradiation method and crushing/step heating to extract halogens. The effects of differing preparation procedures (washing vs acid leaching) and differing analytical procedures have not been documented and may account for the observed discrepancy. For example, if heavy halogens are hosted primarily along grain boundaries in these xenoliths, acid leaching the samples may remove them. Several studies have suggested that grain boundaries are metasomatically enriched in lithophile elements that cannot easily diffuse into minerals (Byerly and Lassiter, 2015; Bedini and Bodinier, 1999; Garrido et al., 2000; Kalfoun et al., 2002; Condie et al., 2004; Harvey et al., 2012). Kilbourne Hole, San Carlos, and Eifel samples are all basalthosted, and so may have experience cryptic grain boundary infiltration from interaction with the host melt. However, grain boundary enrichment can also result from other processes. Byerly and Lassiter, 2015 showed a positive correlation between HFSE enrichment along grain boundaries and clinopyroxene La/Sm in Cerro Chato and Elephant Butte xenoliths, suggesting a metasomatic origin of the grain boundary enrichment, possibly related to Farallonderived fluids/melts. Whether this grain boundary phases host halogens and whether such enrichment results from grain infiltration of the host basalt or from interaction with an earlier

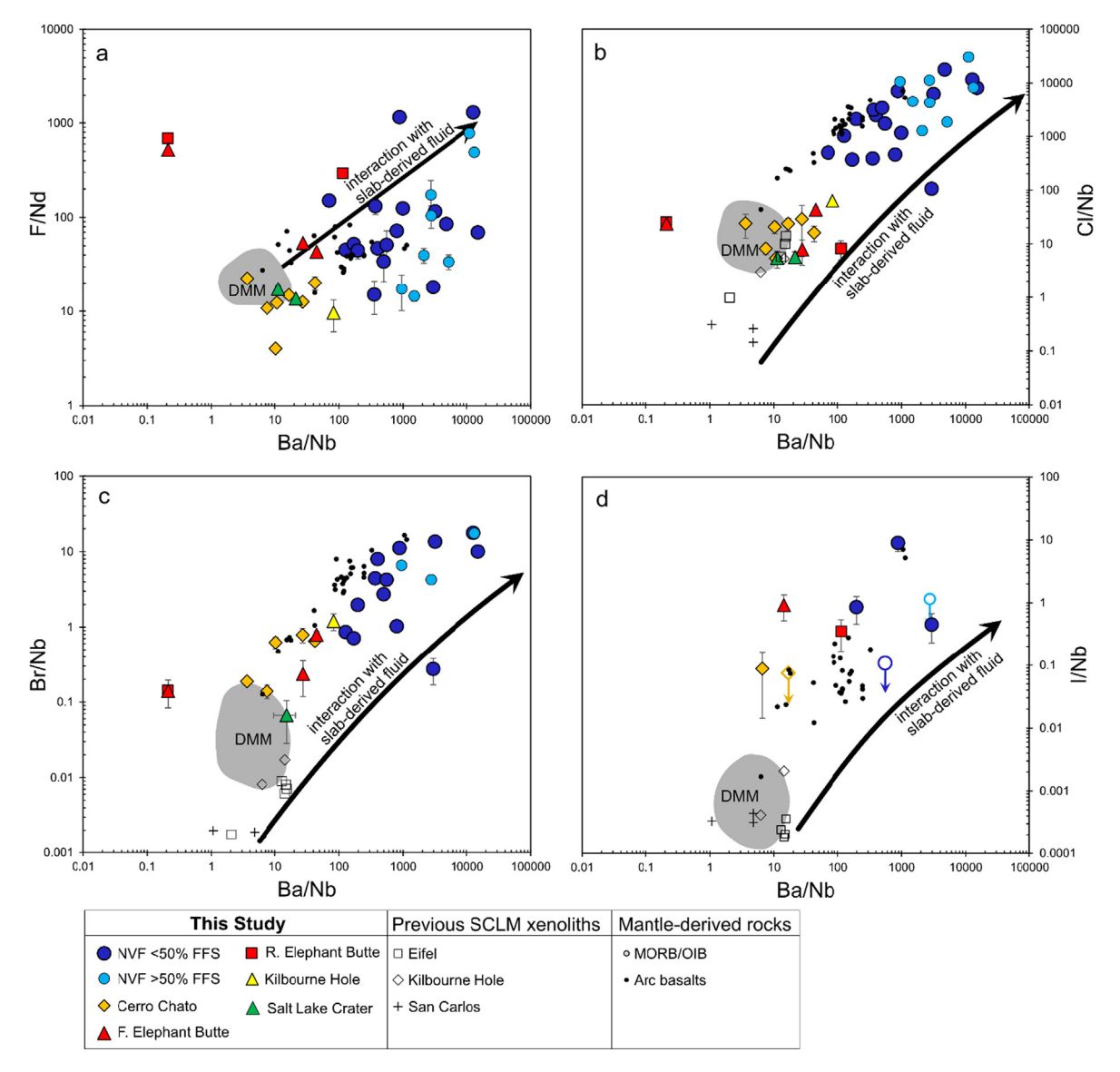


Fig. 5. (a) F/Nd, (b) Cl/Nb, (c) Br/Nb, and (d) I/Nb plotted against Ba/Nb (a proxy for metasomatism from an aqueous fluid). Error bars are 1σ. Broad correlations between Cl/Nb, Br/Nb, and Ba/Nb result from the high Cl, Br, and Ba contents of the modally metasomatized NVF xenoliths and the moderate Cl, Br, and Ba contents of the anhydrous xenoliths from Elephant Butte, Cerro Chato, Kilbourne Hole, San Carlos, and Oahu. Colored open symbols with arrows are data with large blank corrections that are reported as less than maximum values. Average Nb content was calculated for Oahu xenoliths with Br data (see text). NVF = Navajo Volcanic Field, FFS = fracture-filling serpentine (see main text), F. Elephant Butte = Fertile Elephant Butte, R. Elephant Butte = Refractory Elephant Butte, DMM = depleted MORB-source mantle. Gray fields span the range of MORB/OIB values from Kendrick et al. (2017). Xenolith Ba/Nb data from Marshall et al. (2017a), Byerly and Lassiter (2012), and Chatterjee and Lassiter (2016). Previous xenolith data from Kobayashi et al. (2019).

Table 2Olivine oxygen isotope compositions.

Sample Name	δ ¹⁸ O (‰ vs VSMOW)	Sample Name	δ ¹⁸ O (‰ vs VSMOW)
07EB1.01	5.32	EMGN23	5.26 ^a
07EB4.05	5.22	EMGN24	5.15 ^a
07EB1.11	5.34	EMGN27	5.10 ^a
BELB 9-15	5.28, 5.31	EMGN7	5.12 ^a
CC07-1-04	5.10	N106-GN	5.24 ^a
CC07-1-06	5.30	N126-GN	5.21 ^a
CC07-1-20	5.19	N16-GN	5.35 ^a
CC07-1-35	5.41, 5.41	N17-GN	5.08 ^a
CC07-2-1	5.12	N23-GN	5.15 ^a
CC07-3-01	5.36	N55-GN	5.05 ^a
SC23	5.25	N61-GN	5.14 ^a
N51-GN	5.13	EMMR7	5.13 ^a
EMGN2	5.14 ^a	MR-ATG-13	5.28 ^a
EMGN21	5.08 ^a		

Values from this study are from individual analyses; a: Marshall et al. (2017b).

subduction-derived fluid/melt requires further study. However, melt infiltration is likely to be less pervasive in the NVF xenoliths since they are not hosted by silicate melts, but rather by a gassolid mixture (e.g. Smith and Levy, 1976). Grain boundary alteration can still occur in the NVF xenoliths but will result in late serpentine filling fractures (FFS).

Additionally, while the [Br] and Br/Nb of the anhydrous SCLM samples from our study extend from DMM and MORB-like values to higher values, the [Br] and Br/Nb values of Kobayashi et al. (2019) extend to values below DMM and MORB/OIB (Fig. 3c). Such low Br/Nb values are slightly unexpected for SCLM at Eifel and Kilbourne Hole, which are both proposed to have undergone metasomatic enrichment from either a mantle plume or subduction-derived fluid/melt (Perkins et al., 2006; Urann et al., 2017; Wedepohl et al., 1994; Witt-Eickschen et al., 2003; Bekaert et al., 2019, Rizzo et al., 2021). Since mantle plume melts and hydrous fluids/melts are expected to have Br/Nb at least equivalent to

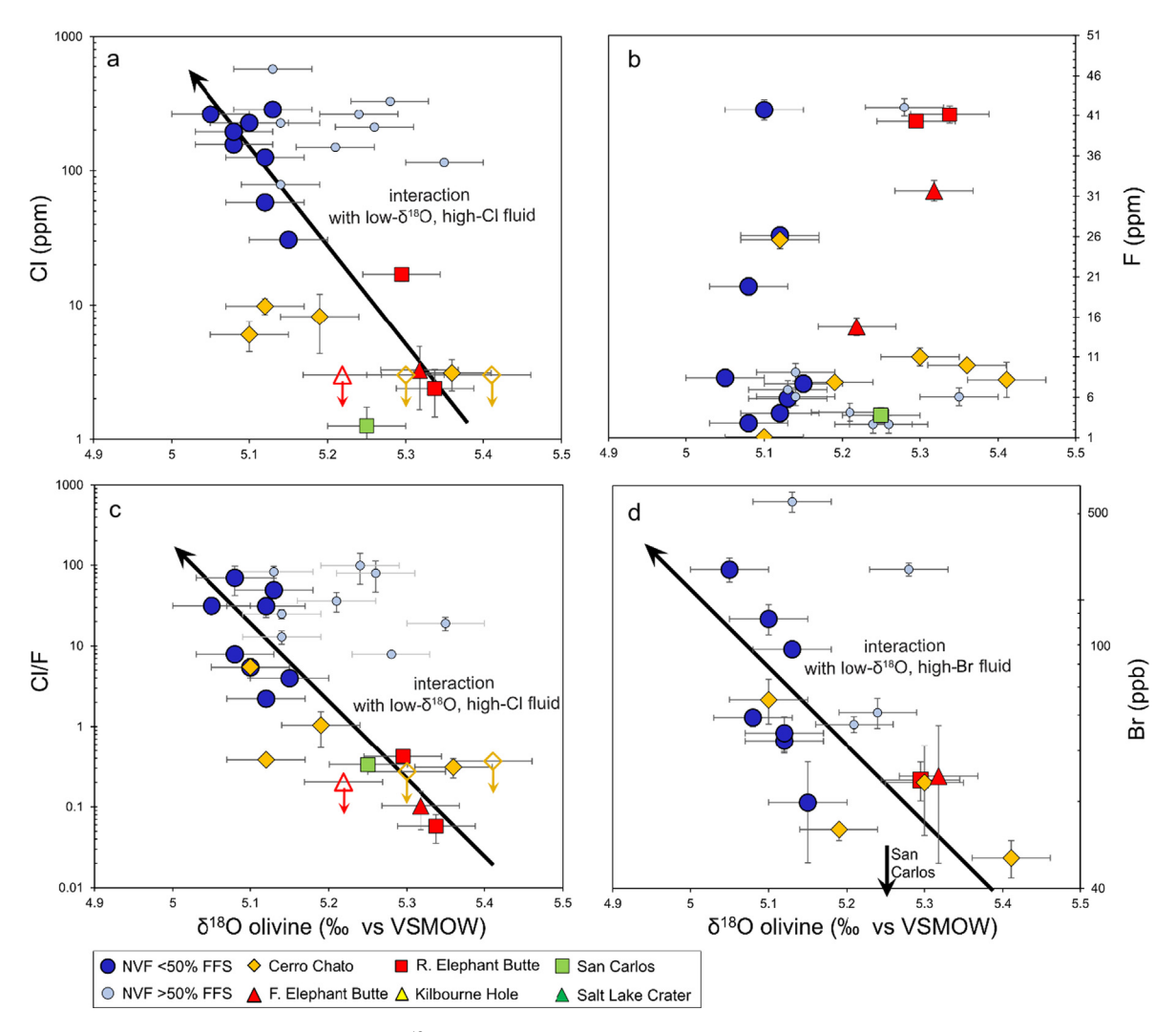


Fig. 6. (a) Cl, (b) F, (c) Cl/F, and (d) Br plotted against olivine δ^{18} O values. Error bars are 1σ . Xenoliths show a correlation between higher [Cl], Cl/F, and [Br] and lower δ^{18} O values but not correlation between F and δ^{18} O values. Late-stage FFS has variably high Cl and Br content without covariation with δ^{18} O values. Colored open symbols with arrows are data with large blank corrections that are reported as maximum values. NVF = Navajo Volcanic Field, FFS = fracture-filling serpentine (see main text), F. Elephant Butte = Fertile Elephant Butte, R. Elephant Butte = Refractory Elephant Butte. NVF δ^{18} O data from Marshall et al. (2017b).

MORB/OIB, Br enrichments should be commensurate with or exceed Nb enrichments, which are 1.1-33 times greater (Kobayashi et al., 2019) than Nb DMM estimates (Salters and Stracke, 2004; Workman and Hart, 2005). As pointed out by Kobayashi et al. (2019), small differences in partition coefficients during melting can cause fractionation between halogens and similarly incompatible trace elements in the depleted residue and may result in lower Br/Nb and Cl/Nb ratios. However, samples from Kilbourne Hole and Eifel are not depleted but rather enriched in incompatible trace elements (Kobayashi et al., 2019), making it unlikely that such Br-Cl-Nb fractionation is occurring. It is plausible that the different sample preparation techniques used by this study and Kobayashi et al. (2019) resulted in analysis of different populations of halogens in the SCLM. Further work must be conducted on the distribution of halogens in mantle xenolith and the effects of various preparation methods. Until that work is done, the reason for the discrepancy between this study and Kobayashi et al. (2019) remains uncertain.

5.2. Halogens in modally metasomatized NVF peridotite xenoliths

Xenoliths from the Navajo Volcanic Field are modally metasomatized and have hydrous minerals that formed *in situ* in the SCLM

prior to eruption (Smith, 2010). While most NVF xenoliths have mantle-like F concentrations, a few of these xenoliths have [F] = 42-47 ppm and F/Nd > 100, significantly higher than canonical mantle values of 11-16 ppm F and F/Nd = 21 (Saal et al., 2002; Salters and Stracke, 2004; Kendrick et al., 2017; Workman et al., 2006). These F contents require some degree of F enrichment. Other Navajo Volcanic Field xenoliths have lower F contents (<2-26 ppm) but elevated F/Nd (>40), similar to the F/Nd of arc basalts (\sim 28–80; Kendrick et al., 2020) (Fig. 3a). It is unlikely that the elevated F/Nd reflect small differences in the partition coefficients of F and Nd during melt depletion of the SCLM, because F is generally more incompatible during mantle melting than Nd (Kendrick et al., 2017), which should result in low F/Nd in melt-depleted residues. Instead, these elevated F/Nd suggest that the NVF SCLM has been moderately enriched in F. The weak correlation between F, LOI, and modal % of hydrous minerals (Fig. 4; Fig. S5) also indicates a metasomatic origin of F.

Unlike the generally mantle-like to minorly enriched F contents, the Cl, Br, and I contents in the Navajo Volcanic Field xenoliths are highly enriched relative to DMM estimates (Fig. 2b-d). The Cl and Br enrichments correlate with low $\delta^{18}O_{olv}$ values and fall at the upper high-halogen end of the general Cl- and Br- $\delta^{18}O_{olv}$ trends (Fig. 6). Oxygen isotopes are a powerful tool for tracing subduction

fluxes into the mantle. Oxygen isotopic fractionations are small at mantle temperatures, resulting in a narrow range of δ^{18} O values from high-temperature processes like partial melting and fractional crystallization. However, water-rock reactions at the surface result in much larger isotopic fractionations. Therefore, if a slabderived fluid interacts with the overlying mantle, it can alter the δ^{18} O values of that mantle. The broad correlation between Cl, Cl/ F, Br and $\delta^{18}O_{olv}$ in NVF, Cero Chato, Elephant Butte, and San Carlos xenoliths indicates a general trend towards lower δ^{18} O values in samples with Cl and Br enrichments. These correlations are likely due to the interaction between the SCLM beneath the Navajo Volcanic Field and a slab-derived fluid with high Cl and Br and low- $\delta^{18}O$ (Fig. 6a,d). The lack of correlation between F and $\delta^{18}O_{olv}$ (Fig. 6b) and the strong negative correlation between Cl/F and δ^{18} -O_{oly} (Fig. 6c) indicates that F is not similarly enriched, suggesting that the slab-derived fluid is poor in F relative to Cl and Br. This result is consistent with Marshall et al. (2017b), who showed a correlation between indices of metasomatism (cpx Ce/Sm) and lower δ¹⁸O_{olv} values in Navajo Volcanic Field xenoliths and interpreted the source of metasomatism to be a Farallon-derived low-δ¹⁸O fluid.

Cl/Nb, Br/Nb, and I/Nb in xenoliths that range up to three orders of magnitude greater than MORB/OIB (Fig. 3b-d) provide further evidence for a Farallon-derived fluid source of the halogens in the NVF SCLM. While the halogens behave like similarly incompatible lithophile elements during melting, the hydrophilic nature of halogens results in their preferential incorporation into aqueous fluids (Manning, 2004), such as those produced during the breakdown of hydrous minerals in the subducted plate. Metasomatism of the SCLM by these fluids results in preferential enrichment in Cl, Br, and I relative to Nb and F relative to Nd. While there are other potential sources of halogen enrichment, such as metasomatism from low-degree melts of the mantle (Gibson et al., 2020), these would also cause enrichment in lithophile elements and result in a positive linear correlation between Cl, Br, and I, and Nb, and F and Nd, as observed in MORB (Fig. 3; Shimizu et al., 2016: Kendrick et al., 2017). Such correlations are not observed in the NVF xenoliths. Therefore, the most likely source of the halogen enrichment is an aqueous fluid derived from the subducted

Decoupling of F from the heavy halogens (Cl, Br, I) in the Navajo Volcanic Field xenoliths (Fig. 2a, c) is also consistent with halogen enrichment from a slab-derived aqueous fluid. Several studies have shown that F is preferentially retained in a dehydrating slab relative to Cl, Br, and I, with an estimated 95% F retention in the subducting slab (Straub and Layne, 2003; Kendrick et al., 2014; Rose-Koga et al., 2017). Cl, Br, and I, however, are more efficiently devolatilized and lost to the overlying mantle, with <10% of Cl and <5% of Br and I remaining in the slab residue (Straub and Layne, 2003; John et al., 2011; Kendrick et al., 2014; Rose-Koga et al., 2017). Such decoupling of F from the other halogens in slabderived fluids is evident from the distinctly higher Cl/F, Br/F, and I/F in arc basalts than in MORB/OIB due to the input of slabderived fluids to the mantle wedge that causes flux melting (Kendrick et al., 2017; Kendrick et al., 2020). Metasomatism by low-degree melts of the mantle can moderately elevate heavy halogen/F due to a higher bulk distribution coefficient of F during mantle melting (Kendrick et al., 2017). However, during melting of both spinel and garnet peridotites, the bulk distribution coefficients of F and Cl are sufficiently similar (Hauri et al., 2006; Dalou et al., 2012) that even extremely low degrees of fractional melting (<1% fractional melting to form Navajo Volcanic Field minettes; Kay and Gast, 1973; Roden, 1981) will not produce the extreme Cl/F (up to 62 in samples with little FFS) observed in these xenoliths. It is plausible that metasomatism of the SCLM by a hydrous melt could fractionate F from the heavy halogens since

hydrous minerals can fractionate halogens during melting or dehydration (Figowy et al., 2021). However, metasomatism by a hydrous melt is still expected to show broad correlations between Cl, Br, and similarly incompatible trace elements, which is not observed (Fig. 2b,c). Therefore, a fluid derived from the dehydration of the subducting Farallon plate is the most likely source of halogen enrichment in these xenoliths.

Additionally, samples with elevated Cl/Nb and Br/Nb also have ratios of fluid-soluble elements to fluid-insoluble elements, such as Ba/Nb that are elevated above DMM values (Fig. 5b,c) which is consistent with a slab-derived fluid source of halogens. This conclusion is also consistent with the interpretations of previous studies (Lee, 2005; Smith, 2010; Marshall et al, 2017b). Enriched fluid-mobile trace element contents in Colorado Plateau SCLM xenoliths paired with bimodal U-Pb zircon ages in Colorado Plateau eclogite xenoliths of Proterozoic age and $\sim 30-80$ Ma, indicate that the fluid-mobile trace element enrichment occurred at $\sim 30-80$ Ma (Lee, 2005). At that time, the Farallon plate was shallowly subducting beneath the Colorado Plateau, and so is the most likely source of the fluid-mobile trace element and halogen enrichment (Lee, 2005; Humphreys et al., 2003).

5.3. Halogens in anhydrous mantle peridotite xenoliths

Chlorine and F concentrations in the anhydrous Cerro Chato, fertile and refractory Elephant Butte, Kilbourne Hole, San Carlos, Eifel, and Hawaii xenolith suites are largely consistent with the DMM (Figs. 2 and 3), suggesting less metasomatic enrichment than the NVF SCLM. Several fertile and refractory Elephant Butte samples have Cl and F contents greater than the highest estimates of DMM (maximum estimates of 16 ppm F and 10 ppm Cl), requiring some degree of halogen enrichment. These high F and Cl samples have Cl/Nb and F/Nd values within the range of MORB and are consistent with Cl/Nb and F/Nd in olivine-hosted melt inclusions from the southern Rio Grande Rift and the Zuni-Banderas Volcanic Field (Fig. 3a, c; Rowe and Lassiter, 2009; Rowe et al., 2015). F/Nd of these xenoliths are similar to previously analyzed SCLM samples (Fig. 3a: Urann et al., 2017: Kobayashi et al., 2019). F contents that are higher than DMM are likely the result of either metasomatism from low-degree melting of the mantle or the incorporation of melt in these peridotite xenoliths along grain boundaries during entrainment and ascent. One fertile and two refractory Elephant Butte samples are exceptions with F/Nd = 290-690. However, these ratios result from exceptionally low bulk rock Nd (0.06–0.14 ppm; Byerly and Lassiter, 2012) instead of enrichments in F.

Salt Lake Crater oceanic lithosphere xenoliths act as a baseline for our measurements of halogens in the lithospheric mantle. The Br contents of these xenoliths are elevated (average = 49 ppb) relative to DMM (~13 ppb; Kendrick et al., 2017) (Figs. 2 and 3). Br/Nb in these xenoliths is also within the MORB/OIB range, indicating that elevated Br contents in Salt Lake Crater xenoliths could be due to a small amount of melt infiltration (Fig. 3c). Additionally, the Salt Lake Crater xenoliths plot close to MORB/OIB in Fig. 5, indicating no subduction-derived halogen enrichment. These data are consistent with Salt Lake Crater xenoliths being oceanic lithosphere that has been metasomatized by Hawaiian melts but not by a subducted component.

Unlike the Salt Lake Crater xenoliths, the Br and I contents of the North American anhydrous xenoliths are enriched. All samples except the San Carlos (<7 ppb Br) xenolith have Br contents higher than DMM (~13 ppb Br; Kendrick et al., 2017). Bromine and I contents are also higher than North American lithospheric mantle measured in previous studies (0.6–8.6 ppb Br and 0.04–0.75 ppb I; Kobayashi et al., 2019). Additionally, the Br contents are decoupled from Cl in most of the anhydrous xenoliths, falling above the global Br-Cl array (Fig. 2b) defined by MORB/OIB. Previous studies

have found significant deviations from the global Br-Cl and I-Cl trends due to metasomatism of the SCLM via slab-derived fluids (Broadley et al., 2016, 2018; Kobayashi et al., 2017), suggesting a slab-derived fluid source of halogen enrichment in the anhydrous xenoliths. Br is also decoupled from Nb and extends from MORBlike Br/Nb to higher Br/Nb (Fig. 3c), indicating that melt infiltration is not responsible for the elevated Br contents. Cryptic grain boundary infiltration of the host melt can also fractionate highly incompatible elements and could fractionate Br, Cl, and Nb. However, cryptic melt infiltration along grain boundaries would also result in elevated Th, U, and Nb contents in the bulk xenoliths (e.g. Bedini and Bodinier, 1999; Harvey et al., 2012). There are no clear correlations between Cl, Br, or Br/Cl and these highly incompatible elements, indicating that melt infiltration along grain boundaries is not the cause of halogen enrichment. Other evidence for a slab-derived fluid source of halogen enrichment comes from the negative correlation (one directional p-values = 0.003-0.06) among [Br], [Cl], Cl/F, and $\delta^{18} O_{olv}$ values that fall along the same trends as the NVF xenoliths (Fig. 6a, c, d).

Several xenoliths from Elephant Butte have interstitial glass that could result in elevated bulk rock halogen contents. However, the glass fraction is small (<1%) and the range of halogen concentrations for Elephant Butte is identical to Cerro Chato, which does not have interstitial glass present. Although incorporation of this glass into the bulk rock analyses may increase the halogen content of some Elephant Butte xenoliths, it is unlikely to significantly alter Br/Cl and Br/Nb at realistic degrees of melting (>1%) due to the similarity in partition coefficients of Br, Cl, and Nb (Kendrick et al., 2017). Therefore, it is unlikely that interstitial glass is responsible for the elevated Br/Cl and Br/Nb in these samples.

5.4. Source of halogens in modally metasomatized NVF peridotite xenoliths

Br/Cl and I/Cl in these xenoliths can constrain the source of the halogen-rich, low- $\delta^{18}O$ fluid that metasomatized the SCLM beneath the Navajo Volcanic Field. Different subducted lithologies, such as serpentinite, altered oceanic crust, sediment, and sedimentary pore fluids, all have different ranges of Br/Cl and I/Cl, whereas DMM has a limited Br/Cl and I/Cl range (Fig. 2; John et al., 2011; Kendrick et al., 2012, 2017). Furthermore, partial melting of the SCLM after enrichment is unlikely to fractionate Cl, Br, and I because of the nearly identical partition coefficients of these halogens during mantle melting (Kendrick et al., 2017).

Navajo Volcanic Field samples have Br/Cl lower than DMM and I/Cl equal to or higher than DMM. These ratios fall slightly below serpentinite Br/Cl and within the altered oceanic crust field (Fig. 7). These ratios could result from halogen enrichment from dehydrating gabbroic altered oceanic crust in the Farallon slab, consistent with a low δ^{18} O signature (Gregory and Taylor, 1981). However, estimates of the depth of the Farallon plate beneath the Colorado Plateau during the Laramide Orogeny are >130 km (West et al., 2004; Smith, 2013), which is deeper than the amphibole- and chlorite-out reactions (Schmidt and Poli, 1998; Hacker, 2008). Since amphibole and chlorite are two of the main halogen hosts in the lower oceanic crust (Barnes and Cisneros, 2012; Kendrick, 2019a, 2019b), it is unlikely that the lower crust in the subducted Farallon plate would retain significant quantities of halogens at depths below that Colorado Plateau and Rio Grande Rift. Therefore, dehydration of the lower oceanic crust in the Farallon plate is unlikely to be source of SCLM halogen enrichment in these xenoliths.

An alternative explanation for the Br/Cl and I/Cl is the dehydration of lithospheric serpentinite in the subducted Farallon plate. The oceanic mantle lithosphere can be serpentinized via the interaction with seawater or sedimentary pore fluids, particularly along

slab-bend fractures (Ranero et al., 2003; Naif et al., 2015; Grevemeyer et al., 2018). Estimates of the degree of oceanic lithospheric mantle serpentinization vary, ranging from 1% to 15% of the uppermost 10 km of the lithospheric mantle (Bloch et al., 2018; Cai et al., 2018; Grevemeyer et al., 2018). Serpentinite in the cold core of a subducting plate can survive to depths below the Colorado Plateau (Ulmer and Trommsdorff, 1995; Schmidt and Poli, 1998; Hacker, 2008; English et al., 2003). Serpentinite can contain Cl, Br, I, and H₂O concentrations that are much higher than altered oceanic crust (Sharp and Barnes, 2004; Scambelluri et al., 2004; Barnes and Sharp, 2006; Kendrick et al., 2011, 2013), but seafloor and mantle wedge serpentinite Br/Cl are higher than Navajo Volcanic Field xenoliths (Fig. 7). However, several studies have shown that dehydration of serpentinite can fractionate Br and I from Cl, resulting in Br/Cl and I/Cl in the devolatilizing fluid that are much higher than the original ratios in the serpentinite (Kendrick et al., 2011, 2018; John et al., 2011). The result is lower Br/Cl and I/Cl in the residual serpentine and in later dehydration fluids (Kendrick et al., 2011, 2018; John et al., 2011). These later dehydration products have virtually identical Br/Cl and I/Cl as the Navajo Volcanic Field samples (Fig. 7). Therefore, dehydration of serpentinized lithospheric mantle that has already undergone partial dehydration is the most likely source of halogen enrichment of the SCLM beneath the Navajo Volcanic Field. Serpentinitederived metasomatism is also consistent with the correlation between low $\delta^{18}O$ and high [CI] and [Br] because serpentinites have $\delta^{18}O$ compositions lower than typical mantle (Wenner and Taylor, 1973).

5.5. Source of halogens in anhydrous North American SCLM

The preferential enrichment in Br (and possibly I) over Cl results in Br/Cl and I/Cl that extend to higher values than any previous reported values in SCLM xenoliths (Figs. 2 and 7). Br/Cl are similar to metasomatized Siberian SCLM xenoliths (Udachnaya), which were proposed to result from metasomatism by subduction-derived fluids (Fig. 2b; Broadley et al., 2018). Additionally, elevated Br/Cl are similar to Canadian cratonic diamonds (Johnson et al., 2000) and eclogite fluid inclusions from the Western Gneiss Region in Norway (Svensen et al., 2001; Hughes et al., 2021).

Additionally, the Br/Cl and I/Cl of the xenoliths are similar to sediment-influenced serpentinite which forms from the hydration of peridotite by sediment-derived fluids (Br/Cl = 0.003-0.013, I/ $Cl = 3x10^{-6}$ -0.0.15), though the xenoliths extend to higher Br/Cl values (Br/Cl = 0.006-0.05; Fig. 7). These elevated Br/Cl values can be explained by fractionation of Br from Cl through complex hydration-dehydration processes, leading to elevated Br/Cl contents due to preferential removal of Cl from the fluid phase, as has been observed in SCLM samples from Canada, Siberia, and Norway (Johnson et al., 2000; Svensen et al., 2001; Hughes et al., 2021). Such processes could increase the Br/Cl ratio of subducted sediment-altered serpentinites to those in Cerro Chato, Kilbourne Hole, and Elephant Butte xenoliths due to crystallization of minor amounts of hydrous minerals (based on Br and Cl contents of SCLM hydrous minerals from Ionov et al., 1997 and Hughes et al., 2021). This suggests that the Farallon-derived fluid metasomatizing the SCLM beneath the Rio Grande Rift and Cerro Chato formed from the dehydration of a subducted serpentinite, similar to the SCLM beneath the Navajo Volcanic Field.

However, for metasomatism from a dehydrating serpentinite to result in the observed Br and Cl contents in these anhydrous SCLM xenoliths, the initial Br and Cl contents of the SCLM prior to metasomatism must have been lower than DMM (\sim 13 ppb Br and \sim 5 ppm Cl) and more similar to the lower Br (\sim 2.4 ppb) and Cl (\sim 0.4 ppm) SCLM concentrations from Kobayashi et al. (2019) and Urann et al. (2017). The black curves in Fig. 7 are

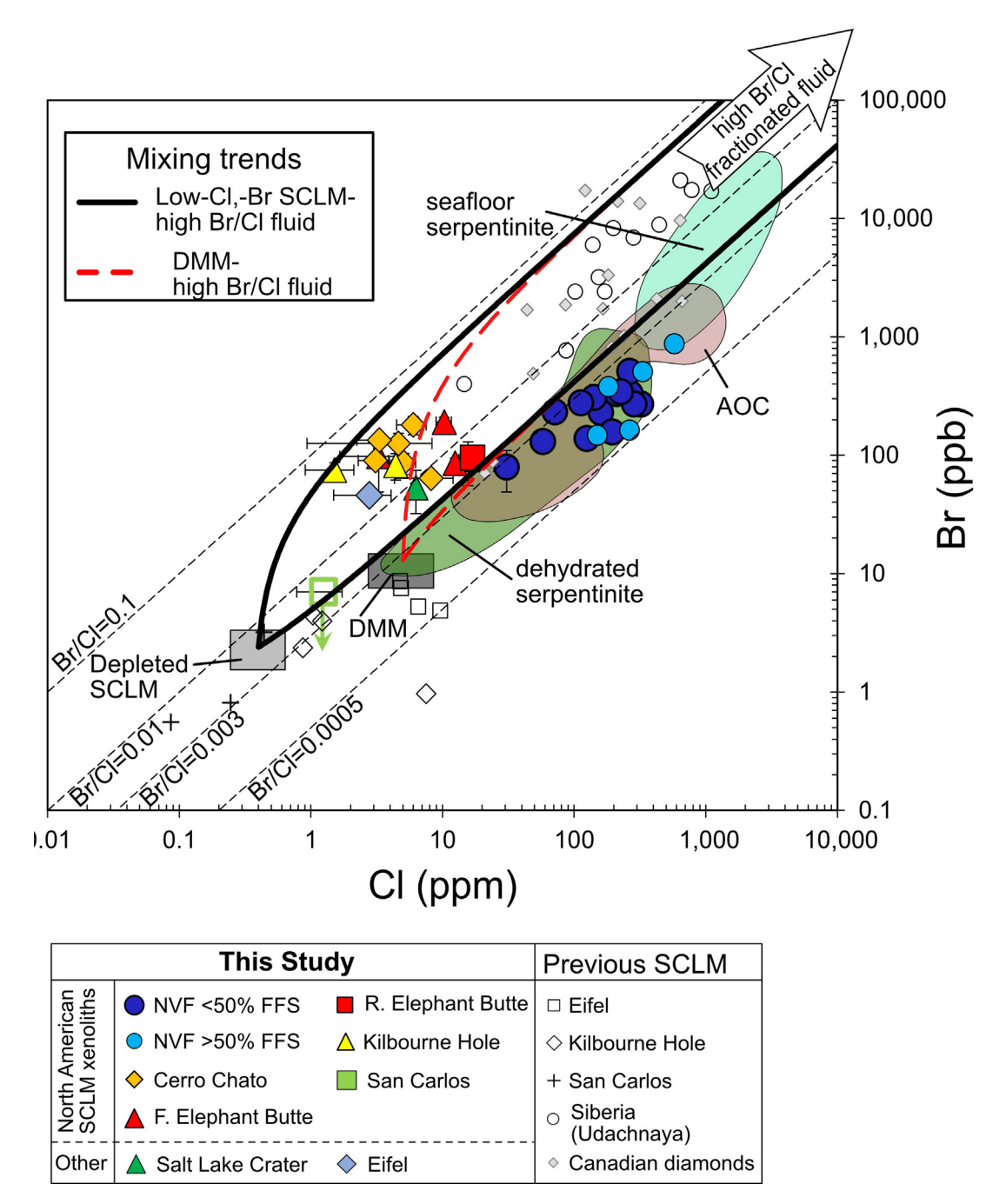


Fig. 7. Br plotted against Cl. Error bars are 1σ. NVF = Navajo Volcanic Field, FFS = fracture-filling serpentine (see main text), F. Elephant Butte = Fertile Elephant Butte, R. Elephant Butte = Refractory Elephant Butte, AOC = altered oceanic crust, DMM = depleted MORB-source mantle. The two black curves are mixing trends between SCLM with highly depleted halogen contents (see text) and a sediment-altered serpentinite with high Br/Cl = 0.004 and 0.074 based on Hughes et al. (2021). The two red curves are mixing trends between average DMM and the high Br/Cl sediment-altered serpentinite. DMM range from Kendrick et al. (2017). Previous SCLM data from Kobayashi et al. (2019), Broadley et al. (2018), and Johnson et al. (2000). High Br/Cl fractionated fluid ranges based on Hughes et al. (2021). AOC data from Kendrick (2019a,b) and Chavrit et al. (2016). Dehydrated serpentinite data from Kendrick et al. (2011) and John et al. (2011). Seafloor serpentinite data from Kendrick et al. (2013). (For interpretation of the references to colour in this figure legend, the reader is referred to the web version of this article.)

mixing curves between a halogen-depleted SCLM (0.4 ppm Cl and 2.4 ppb Br) and high Br/Cl fluid derived from sediment-influenced serpentinite, whereas the red dashed curves are mixing sediment-influenced serpentinite and DMM. The Br/Cl values of the serpentinite endmember are based on other high-Br/Cl fluids from Johnson et al. (2000), Svensen et al. (2001), and Hughes et al. (2021) that have undergone fractionation of Br from Cl. Metasomatism of SCLM with initially DMM-like Cl and Br content can produce the Br and Cl content of a few Elephant Butte and Cerro Chato samples but cannot produce the Br and Cl contents in most

Cerro Chato and Kilbourne Hole samples. If the SCLM starts with a more halogen-depleted composition similar to that observed for the San Carlos xenolith from this study and the Kilbourne Hole and San Carlos samples from Kobayashi et al. (2019) and Urann et al. (2017) (average = 2.4 ppb Br and 0.4 ppb Cl), then the entire Cl and Br range of all Cerro Chato, Kilbourne Hole, and Elephant Butte can be explained by the addition of a serpentinite-derived fluid. Therefore, the SCLM beneath the Colorado Plateau and Rio Grande Rift was likely highly depleted in halogens prior to metasomatism from the Farallon slab.

The reason for the difference in Farallon-derived Br/Cl and I/Cl between these anhydrous xenoliths and the modally hydrated xenoliths is unclear. The localities are all approximately the same distance from the paleo-trench but are spread out orthogonally to the motion of the subducting Farallon plate (Fig. 1b). The difference in subduction-signature could then be related to spatial variability in the source of the fluid serpentinizing the Farallon mantle prior to its subduction. Hydration on the seafloor or along slabbend faults of the northern portion of the Farallon plate by seawater would impart the observed Br/Cl signature in the NVF xenoliths, whereas hydration by fluids that had interacted with sediment would account for the elevated Br/Cl in Cerro Chato, Kilbourne Hole, and Elephant Butte xenoliths. Such variability is possible if there are significant differences in the sediment thickness above the subducting plate.

6. Implications on global halogen content

Extrapolation of results from the SCLM localities in this study to SCLM in general is difficult given that the metasomatic conditions of the Colorado Plateau and Rio Grande Rift lithosphere may not be generally applicable to all metasomatized SCLM. However, because samples in this study have experienced such high degrees of metasomatic halogen enrichment, extrapolation of the halogen enrichment in these xenoliths to all metasomatized SCLM provides an upper estimate of the halogen content of the global SCLM. The average halogen contents of metasomatized SCLM xenoliths from Navajo Volcanic Field (only samples without significant FFS), Cerro Chato, Elephant Butte, and Eifel are listed in Table 3. Due to the large error in I measurements on these xenoliths, extrapolation of I contents of these xenoliths is not attempted. Averaging these halogen contents produces a metasomatized SCLM with 14 ppm F, 47 ppm Cl, and 122 ppb Br. Additionally, the halogen abundances of San Carlos and the required mixing lines in Fig. 7a suggest that unmetasomatized SCLM contains relatively low Cl, Br, and I concentrations similar to those from Kobayashi et al. (2019) (see Table 3). Assuming the sub-continental lithospheric mantle is 2% of the primitive mantle (McDonough, 1990; Pearson and Nowell, 2002), the total quantity of halogens in the SCLM can be approximated based on the assumed proportion of metasomatized SCLM. Taking two endmember scenarios: 5% and 90% of global SCLM is metasomatized by subducted plates, the global SCLM would contain $(1.0-1.3) \times 10^{18}$ kg F, $(2-34) \times 10^{17}$ kg Cl, and $(0.7-9) \times 10^{15}$ kg Br. These ranges are equivalent to 3-4%, 3-40%, and 2-24% of current DMM estimates for masses of F, Cl, and Br, respectively (Kendrick et al., 2017). Additionally, the calculated total fraction of the Bulk Silicate Earth halogen content is relatively small for F (1.4-1.8%), Cl (0.2-3.3%), and Br (0.2-2.8%) compared to halogen reservoirs like DMM (\sim 50% BSE F) and seawater (\sim 25% and \sim 30% BSE Cl and Br, respectively). While subduction-related metasomatism of the SCLM overall has only a minor effect on the BSE halogen budget, it can have a large impact on estimates of the Cl and Br bulk concentration of the mantle. More work is needed on bulk peridotite and pyroxenite SCLM xenolith halogen contents from other localities to better refine these values.

7. Conclusions

Our study of the bulk rock halogen content and $\delta^{18}O_{olv}$ values of lithospheric mantle xenoliths indicates that fluids derived from dehydrating slab-core serpentinites in the Farallon plate metasomatized the SCLM beneath the Colorado Plateau and Rio Grande Rift. This metasomatism resulted in large enrichment in Br and I, variable enrichment in Cl, and minor to no enrichment in F. This slab-derived metasomatic halogen enrichment of the SCLM is not isolated to the modally hydrated SCLM beneath the Navajo Volcanic Field, but rather is laterally extensive below the Colorado Plateau and Rio Grande Rift as far as 1000 km inboard from the trench. The lack of correlation between modal hydrous mineral abundance and halogen content across these xenolith suites broadly indicates that halogen metasomatism does not need to correlate with hydration.

Flat-slab subduction of the Farallon plate caused direct contact between the North American SCLM and the subducting plate. This contact allowed for a more direct transfer of halogens from the Farallon plate to the North American SCLM due to the lack of an asthenospheric mantle wedge. As such, the SCLM in this study represents an extreme endmember in the extent of halogen enrichment. Taking these endmember compositions and applying them to global SCLM provides an upper estimate for the total mass of halogen in global SCLM of 3–4%, 3–40%, and 2–24% of the current halogen mass estimates of F, Cl, and Br in the depleted mantle. These results demonstrate that subduction-derived Cl and Br in the SCLM can be extensive and should be considered in halogen mass balance calculations.

Declaration of Competing Interest

The authors declare that they have no known competing financial interests or personal relationships that could have appeared to influence the work reported in this paper.

Acknowledgements

This work is supported by funding by NSF-EAR-1850749 to J.D. B. and J.C.L. We would like to thank Ben Byerly for his work collecting oxygen isotope data, Matthew Riley for collected XRD data, and Doug Smith for fielding questions about samples from the Colorado Plateau. This work uses samples that were previously collected on Navajo Lands, with permission from the Navajo Nation. This manuscript benefitted from insightful and constructive comments by Sally Gibson, Michael Rowe, two anonymous reviewers, and editor Janne Blichert-Toft.

Table 3 Estimated abundances of halogens in SCLM.

	Cl (ppm)	F (ppm)	Br (ppb)	I (ppb)
Navajo Volcanic Field	177	12	249	207
Cerro Chato	5	12	131	35
Rio Grande Rift	5	32	72	87
Eifel Volcanic Field	3	8	46	81
Av. metasom. SCLM	47	16	124	102
Av. unmetasom. SCLM	0.4	12	2.4	0.5
Halogen mass in global SCLM*	Cl (g $\times 10^{20}$)	$F(g \times 10^{21})$	Br (g $\times 10^{18}$)	$I(g \times 10^{17})$
5% metasom. SCLM	2	1.0	0.7	5
90% metasom. SCLM	34	1.3	9	75

^{*} Based on SCLM mass equal to 2% primitive mantle mass.

Appendix A. Supplementary material

The supplementary material includes representative photomicrographs from different xenolith localities, a description of the fracture-filling serpentine in the xenoliths, modal abundance estimates of hydrous minerals in the modally hydrated Navajo Volcanic Field xenoliths, and discussions of sample duplicate reproducibility, inter-lab reproducibility, and halogen contamination from vanadium pentoxide flux. Additionally, a table including the data from this study is included in the supplementary material entitled "Research Data". This table also includes previously published data from Marshall et al. (2017a, 2017b), Byerly and Lassiter (2012) and Chatterjee and Lassiter (2016), to which the data from this study are compared (e.g. Ba/Nb, LOI). Supplementary material to this article can be found online at https://doi.org/10.1016/j.gca.2023.03.014.

References

- Bachman, G.O., Mehnert, H.H., 1978. New K-Ar dates and the late Pliocene to Holocene geomorphic history of the central Rio Grande region. New Mex. Geol. Soc. Am. Bull. 89, 283–292.
- Baldridge, W.S., 1979. Mafic and ultramafic inclusion suites from the Rio-Grande Rift (New-Mexico) and their bearing on the composition and thermal state of the lithosphere. J. Volcanol. Geothermal Res. 6, 319–351.
- Baldridge, W.S., Damon, P.E., Shafiqullah, M., Bridwell, R.J., 1980. Evolution of the central Rio Grande rift, New Mexico: New potassium-argon ages. Earth Planet. Sci. Lett. 51 (2), 309–321.
- Barnes, J.D., Cisneros, M., 2012. Mineralogical control on the chlorine isotope composition of altered oceanic crust. Chem. Geol. 326–327, 51–60.
- Barnes, J.D., Sharp, Z.D., 2006. A chlorine isotope study of DSDP/ODP serpentinized ultramafic rocks: insights into the serpentinization process. Chem. Geol. 228, 246–265
- Barnes, J.D., Manning, C.E., Scambelluri, M., Selverstone, J., 2018. Behavior of halogens during subduction zone processes. In: Harlov, D.E., Aranovich, L. (Eds.), The Role of Halogens in Terrestrial and Extraterrestrial Geochemical Processes. Springer, Cham, pp. 545–590.
- Bedini, R.M., Bodinier, J.L., 1999. Distribution of incompatible trace elements between the constituents of spinel peridotite xenoliths: ICP-MS data from the East African Rift. Geochim. Cosmochim. Acta 63 (22), 3883–3900.
- Behr, W.M., Smith, D., 2016. Deformation in the mantle wedge associated with Laramide flat-slab subduction. Geochem. Geophys. Geosyst. 17 (7), 2643–2660.
- Bekaert, D.V., Broadley, M.W., Caracausi, A., Marty, B., 2019. Novel insights into the degassing history of Earth's mantle from high precision noble gas analysis of magmatic gas. Earth Planet. Sci. Lett. 525, 115766.
- Bekaert, D.V., Turner, S.J., Broadley, M.W., Barnes, J.D., Halldórsson, S.A., Labidi, J., Wade, J., Walowski, K.J., Barry, P.H., 2021. Subduction-driven volatile recycling: A global mass balance. An. Rev. Earth Planet. Sci. 49, 37–70.
- Bernard, R.E., Behr, W.M., Becker, T.W., Young, D.J., 2019. Relationships between olivine CPO and deformation parameters in naturally deformed rocks and implications for mantle seismic anisotropy. Geochem. Geophys. Geosyst. 20, 3469–3494.
- Bernini, D., Wiedenbeck, M., Dolejš, D., Keppler, H., 2013. Partitioning of halogens between mantle minerals and aqueous fluids: implications for the fluid flow regime in subduction zones. Contrib. Mineral. Petrol. 165, 117–128.
- Beyer, C., Klemme, S., Wiedenbeck, M., Stracke, A., Vollmer, C., 2012. Fluorine in nominally fluorine-free mantle minerals: Experimental partitioning of F between olivine, orthopyroxene and silicate melts with implications for magmatic processes. Earth Planet. Sci. Lett. 337, 1–9.
- Bizimis, M., Griselin, M., Lassiter, J.C., Salters, V.J.M., Sen, G., 2007. Ancient recycled mantle lithosphere in the Hawaiian plume: Osmium-Hafnium isotopic evidence from peridotite mantle xenoliths. Earth Planet. Sci. Lett. 257, 259–273.
- Bloch, W., John, T., Kummerow, J., Salazar, P., Krüger, O.S., Shapiro, S.A., 2018. Watching dehydration: seismic indication for transient fluid pathways in the oceanic mantle of the subducting Nazca Slab. Geochem. Geophys. Geosyst. 19, 3189–3207
- Broadley, M.W., Ballentine, C.J., Chavrit, D., Dallai, L., Burgess, R., 2016. Sedimentary halogens and noble gases within Western Antarctic xenoliths: Implications of extensive volatile recycling to the sub continental lithospheric mantle. Geochim. Cosmochim. Acta 176, 139–156.
- Broadley, M.W., Barry, P.H., Ballentine, C.J., Taylor, L.A., Burgess, R., 2018. End-Permian extinction amplified by plume-induced release of recycled lithospheric volatiles. Nature Geosci. 11, 682–687.
- Broadley, M.W., Sumino, H., Graham, D.W., Burgess, R., Ballentine, C.J., 2019. Recycled components in mantle plumes deduced from variations in halogens (Cl, Br, and I), trace elements, and ³He/⁴He along the Hawaiian-Emperor Seamount Chain. Geochem. Geophys. Geosyst. 20, 277–294.
- Bu, X., Wang, T., Hall, G., 2003. Determination of halogens in organic compounds by high resolution inductively coupled plasma mass spectrometry (HR-ICP-MS). J. Anal. At. Spectrom. 18, 1443–1451.

- Burgess, R., Layzelle, E., Turner, G., Harris, J.W., 2002. Constraints on the age and halogen composition of mantle fluids in Siberian coated diamonds. Earth Planet. Sci. Lett. 197, 193–203.
- Bussod, G.Y.A., Williams, D.R., 1991. Thermal and kinematic model of the southern Rio Grande Rift: inferences from crustal and mantle xenoliths From Kilbourne Hole, New Mexico. Tectonophysics 197, 373–389.
- Byerly, B.L., Lassiter, J.C., 2012. Evidence from mantle xenoliths for lithosphere removal beneath the Central Rio Grande Rift. Earth Planet. Sci. Lett. 355–356, 82–93
- Byerly, B.L., Lassiter, J.C., 2014. Isotopically ultra-depleted domains in the convecting upper mantle: Implications for MORB petrogenesis. Geology 42, 203–206.
- Byerly, B.L., Lassiter, J.C., 2015. Trace element partitioning and Lu-Hf isotope systematics in spinel peridotites from the Rio Grande Rift and Colorado Plateau: Towards improved age assessment of clinopyroxene Lu/Hf-¹⁷⁶Hf/¹⁷⁷Hf in SCLM peridotite. Chem. Geol. 413, 146–158.
- Cai, C., Wiens, D.A., Shen, W., Eimer, M., 2018. Water input into the Mariana subduction zone estimated from ocean-bottom seismic data. Nature 563, 389–392
- Chapin, C.E., 1979. Evolution of the Rio Grande Rift a Summary. In: Riecker, R.E. (Ed.), Rio Grande rift: tectonics and magmatism. American Geophysical Union, Washington D.C, pp. 1–5.
- Chatterjee, R., Lassiter, J.C., 2016. ¹⁸⁶Os/¹⁸⁸Os variations in upper mantle peridotites: Constraints on the Pt/Os ratio of primitive upper mantle, and implications for late veneer accretion and mantle mixing timescales. Chem. Geol. 442, 11–22.
- Chavrit, D., Burgess, R., Sumino, H., Teagle, D.A.H., Droop, G., Shimizu, A., Ballentine, C.J., 2016. The contribution of hydrothermally altered ocean crust to the mantle halogen and noble gas cycles. Geochim. Cosmochim. Acta 183, 106–124.
- Chazot, G., Lowry, D., Menzies, M., Mattey, D., 1997. Oxygen isotopic composition of hydrous and anhydrous mantle peridotites. Geochim. Cosmochim. Acta 61 (1), 161–169.
- Chu, L., Enggist, A., Luth, R.W., 2011. Effect of KCl on melting in the Mg₂SiO₄–MgSiO₃–H₂O system at 5 GPa. Contrib. Mineral. Petrol. 162, 565–571.
- Clague, D.A., Frey, F.A., 1982. Petrology and trace element chemistry of the Honolulu volcanics, Oahu: implication for the oceanic mantle below Hawaii. J. Petrol. 23, 447–504.
- Condie, K.C., Cox, J., O'Reilly, S.Y., Griffin, W.L., Kerrich, R., 2004. Distribution of high field strength and rare earth elements in mantle and lower crustal xenoliths from the southwestern United States: the role of grain-boundary phases. Geochim. Cosmochim. Acta 68 (19), 3919–3942.
- Dalou, C., Koga, K.T., Shimizu, N., Boulon, J., Devidal, J.-L., 2012. Experimental determination of F and Cl partitioning between lherzolite and basaltic melt. Contrib. Mineral. Petrol. 163, 591–609.
- Dickinson, W.R., Snyder, W.S., 1978. Plate tectonics of the Laramide orogeny. In: Matthews, V. (Ed.), Laramide Folding Associated with Basement Block Faulting in the Western United States. The Geological Society of America Inc., Memoirs 151. Boulder, pp. 355–366.
- English, J.M., Johnston, S.T., Wang, K., 2003. Thermal modelling of the Laramide orogeny: Testing the flat-slab subduction hypothesis. Earth Planet. Sci. Lett. 214, 619–632.
- Figowy, S., Dubacq, B., D'Arco, P., 2021. Crystal chemistry and partitioning of halogens in hydrous silicates. Contrib. Mineral. Petrol. 176, 100.
- Filiberto, J., Wood, J., Dasgupta, R., Shimizu, N., Le, L., Treiman, A.H., 2012. Effect of fluorine on near-liquidus phase equilibria of an Fe–Mg rich basalt. Chem. Geol. 312–313. 118–126.
- Filiberto, J., Dasgupta, R., Gross, J., Treiman, A.H., 2014. Effect of chlorine on near-liquidus phase equilibria of an Fe–Mg-rich tholeitic basalt. Contrib. Mineral. Petrol. 168, 1027.
- Frey, F.A., Prinz, M., 1978. Ultramafic inclusions from San Carlos, Arizona: petrologic and geochemical data bearing on their petrogenesis. Earth Planet. Sci. Lett. 38, 129–176.
- Frezzotti, M.L., Ferrando, S., 2018. The role of halogens in the lithospheric mantle. In: Harlov, D.E., Aranovich, L. (Eds.), The Role of Halogens in Terrestrial and Extraterrestrial Geochemical Processes. Springer, Cham, pp. 805–845.
- Gao, W., Grand, S.P., Baldridge, W.S., Wilson, D., West, M., Ni, J.F., Aster, R., 2004. Upper mantle convection beneath the central Rio Grande rift imaged by P and S wave tomography. J. Geophys. Res. 109, B03305.
- Garrido, C.J., Bodinier, J.-L., Alard, O., 2000. Incompatible trace element partitioning and residence in anhydrous spinel peridotites and websterites from the Ronda orogenic peridotite. Earth Planet. Sci. Lett. 181 (3), 341–358.
- Gibson, S.A., Rooks, E.E., Day, J.A., Petrone, C.M., Leat, P.T., 2020. The role of subcontinental mantle as both "sink" and "source" in deep Earth volatile cycles. Geochim. Cosmochim. Acta 275, 140–162.
- Gregory, R.T., Taylor Jr., H.P., 1981. An oxygen isotope profile in a section of Cretaceous oceanic crust, Samail ophiolite, Oman: evidence for ¹⁸O buffering of the oceans by deep (>5km) seawater- hydrothermal circulation at mid-ocean ridges. J. Geophys. Res. 86, 2737–2755.
- Grevemeyer, I., Ranero, C.R., Ivandic, M., 2018. Structure of oceanic crust and serpentinization at subduction trenches. Geosphere 14 (2), 395–418.
- Hacker, B.R., 2008. H₂O subduction beyond arcs. Geochem. Geophys. Geosyst. 9 (3), 003001.
- Hanley, J.J., Koga, K.T., 2018. Halogens in terrestrial and cosmic geochemical systems: abundances, geochemical behaviors, and analytical methods. In: Harlov, D.E., Aranovich, L. (Eds.), The Role of Halogens in Terrestrial and Extraterrestrial Geochemical Processes. Springer, Cham, pp. 21–121.

- Harvey, J., Yoshikawa, M., Hammond, S.J., Burton, K.W., 2012. Deciphering the trace element characteristics in Kilbourne Hole peridotite xenoliths: Melt-rock interaction and metasomatism beneath the Rio Grande Rift, SW USA. J. Petrol. 53 (8), 1709–1742.
- Hauri, E.H., Gaetani, G.A., Green, T.H., 2006. Partitioning of water during melting of the Earth's upper mantle at $\rm H_2O$ undersaturated conditions. Earth Planet. Sci. Lett. 248, 715–734.
- Hughes, L., Cuthbert, S., Quas-Cohen, A., Ruzié-Hamilton, L., Pawley, A., Droop, G., Lyon, I., Tartèse, R., Burgess, R., 2021. Halogens in Eclogite Facies Minerals from the Western Gneiss Region, Norway. Minerals 11 (7), 760.
- Humphreys, E.D., 1995. Post-Laramide removal of the Farallon slab, western United States. Geology 23, 987–990.
- Humphreys, E., 2009. Relation of flat subduction to magmatism and deformation in the western United States. In: Kay, S.M., Ramos, V.A., Dickinson, W.R. (Eds.), Backbone of the Americas: Shallow Subduction, Plateau Uplift, and Ridge and Terrane Collision. The Geological Society of America Inc., Memoirs 204, Boulder, pp. 85–98.
- Humphreys, E., Hessler, E., Dueker, K., Farmer, G.L., Erslev, E., Atwater, T., 2003. How Laramide-age hydration of North American lithosphere by the Farallon Slab controlled subsequent activity in the western United States. Int. Geol. Rev. 45, 575-595.
- Ionov, D.A., Griffin, W.L., O'Reilly, S.Y., 1997. Volatile-bearing minerals and lithophile trace elements in the upper mantle. Chem. Geol. 141 (3–4), 153–184.
- Jochum, K.P., Weis, U., Schwager, B., Stoll, B., Wilson, S.A., Haug, G.H., Andreae, M.O., Enzweiler, J., 2015. Reference values following ISO guidelines for frequently requested rock reference materials. Geostandards Geoanal. Res. 40 (3), 333– 350.
- John, T., Scambelluri, M., Frische, M., Barnes, J.D., Bach, W., 2011. Dehydration of subducting serpentinite: Implications for halogen mobility in subduction zones and the deep halogen cycle. Earth Planet. Sci. Lett. 308, 65–76.
- Johnson, L.H., Burgess, R., Turner, G., Milledge, H.J., Harris, J.W., 2000. Noble gas and halogen geochemistry of mantle fluids: Comparison of African and Canadian diamonds. Geochim. Cosmochim. Acta 64 (4), 717–732.
- Kalfoun, F., Ionov, D., Merlet, C., 2002. HFSE residence and Nb/Ta ratios in metasomatised, rutile-bearing mantle peridotites. Earth Planet. Sci. Lett. 199 (1–2), 49–65.
- Kay, R.W., Gast, P.W., 1973. The rare earth content and origin of alkali rich basalts. J. Geol. 81, 653–682.
- Kendrick, M.A., 2019a. Halogens in Atlantis Bank gabbros, SW Indian Ridge:
 Implications for styles of seafloor alteration. Earth Planet. Sci. Lett. 514, 96–107.
 Kendrick, M.A., 2019b. Halogens in altered ocean crust from the East Pacific Rise
- (ODP/IODP Hole 1256D). Geochim. Cosmochim. Acta 261, 93–112. Kendrick, M.A., Scambelluri, M., Honda, M., Phillips, D., 2011. High abundances of noble gas and chlorine delivered to the mantle by serpentinite subduction.
- Nature Geosci. 4 (11), 807–812. Kendrick, M.A., Kamenetsky, V.S., Phillips, D., Honda, M., 2012. Halogen systematics (Cl, Br, I) in Mid-Ocean Ridge Basalts: A Macquarie Island case study. Geochim. Cosmochim. Acta 81, 82–93.
- Kendrick, M.A., Honda, M., Pettke, T., Scambelluri, M., Phillips, D., Giuliani, A., 2013. Subduction zone fluxes of halogens and noble gases in seafloor and forearc serpentinites. Earth Planet. Sci. Lett. 365, 86–96.
- Kendrick, M.A., Jackson, M.G., Kent, A.J.R., Hauri, E.H., Wallace, P.J., Woodhead, J., 2014. Contrasting behaviours of CO₂, S, H₂O and halogens (F, Cl, Br, and I) in enriched-mantle melts from Pitcairn and Society seamounts. Chem. Geol. 370, 69–81.
- Kendrick, M.A., Hémond, C., Kamenetsky, V.S., Danyushevsky, L., Devey, C.W., Rodermann, T., Jackson, M.G., Perfit, M.R., 2017. Seawater cycled throughout Earth's mantle in partially serpentinized lithosphere. Nature Geosci. 10, 222– 227.
- Kendrick, M.A., Scambelluri, M., Hermann, J., Padron-Navarta, J.A., 2018. Halogens and noble gases in serpentinites and secondary peridotites: Implications for seawater subduction and the origin of mantle neon. Geochim. Cosmochim. Acta 235, 285–304.
- Kendrick, M.A., Danyushevsky, L.V., Falloon, T.J., Woodhead, J.D., Arculus, R.J., Ireland, T., 2020. SW Pacific arc and backarc lavas and the role of slab-bend serpentinites in the global halogen cycle. Earth Planet. Sci. Lett. 530, 115921.
- Kobayashi, M., Sumino, H., Nagao, K., Ishimaru, S., Arai, S., Yoshikawa, M., Kawamoto, T., Kumagai, Y., Kobayashi, T., Burgess, R., Ballentine, C.J., 2017. Slab-derived halogens and noble gases illuminate closed system processes controlling volatile element transport into the mantle wedge. Earth and Planet. Sci. Lett. 457, 106–116.
- Kobayashi, M., Sumino, H., Burgess, R., Nakai, S., Iizuka, T., Nagao, J., Kagi, H., Nakamura, M., Takahashi, E., Kogiso, T., Ballentine, C., 2019. Halogen heterogeneity in the lithosphere and evolution of mantle halogen abundances inferred from intraplate mantle xenoliths. Geochem. Geophys. Geosyst. 20, 952–973.
- Lassiter, J.C., Byerly, B.L., Snow, J.E., Hellebrand, E., 2014. Constraints from Osisotope variations on the origin of Lena Trough abyssal peridotites and implications for the composition and evolution of the depleted upper mantle. Earth Planet. Sci. Lett. 403, 178–187.
- Laughlin, A.W., Aldrich, M.J., Shafiqullah, M., Husler, J., 1986. Tectonic implications of the age, composition, and orientation of lamprophyre dikes, Navajo volcanic field, Arizona. Earth Planet. Sci. Lett. 76, 361–374.
- Laughlin, A.W., Perry, F.V., Damon, P.E., Shafiqullah, M., WoldeGabriel, G., McIntosh, W.C., Harrington, C.D., Wells, S.G., Drake, P.G., 1993. Geochronology of Mount

- Taylor, Cebollita Mesa, and Zuni-Bandera volcanic fields, Cibola County, New Mexico. N. M. Geol. 15. 81–92.
- Lawton, T.F., McMillan, N.J., 1999. Arc abandonment as a cause for passive continental rifting: comparison of the Jurassic Mexican Borderland rift and the Cenozoic Rio Grande rift. Geology 27, 779–782.
- Le Voyer, M., Cottrell, E., Kelley, K.A., Brounce, M., Hauri, E.H., 2015. The effect of primary versus secondary processes on the volatile content of MORB glasses: An example from the equatorial Mid-Atlantic Ridge (5°N–3°S). J. Geophys. Res. Sol. Earth 120, 125–144.
- Lee, C.-T.-A., 2005. Trace element evidence for hydrous metasomatism at the base of the North American lithosphere and possible association with Laramide lowangle subduction. J. Geol. 113, 673–685.
- Mack, G.H., Nightengale, A.L., Seager, W.R., Clemons, R.E., 1994. The Oligocene Goodsight-Cedar Hills half graben near Las Cruces and its implications to the evolution of the Mogollon-Datil volcanic field and to the southern Rio Grande rift. New Mex. Geol. Soc. Guidebook 45, 135–142.
- Manning, C.E., 2004. The chemistry of subduction-zone fluids. Earth Planet. Sci. Lett. 223. 1–16.
- Marshall, E.W., Lassiter, J.C., Barnes, J.D., Luguet, A., Lissner, M., 2017a. Mantle melt production during the 1.4 Ga Laurentian magmatic event: Isotopic constraints from Colorado Plateau mantle xenoliths. Geology 45 (6), 519–522.
- Marshall, E.W., Barnes, J.D., Lassiter, J.C., 2017b. The role of serpentinite-derived fluids in metasomatism of the Colorado Plateau (USA) lithospheric mantle. Geology 45 (12), 1–4.
- Marshall, E., Lassiter, J.C., Barnes, J.D., 2018. On the (mis)behavior of water in the mantle: controls on nominally anhydrous mineral water contents in mantle peridotites. Earth Planet. Sci. Lett. 499, 219–229.
- Mattey, D., Lowry, D., Macpherson, C., 1994. Oxygen isotope composition of mantle peridotite. Earth Planet. Sci. Lett. 128, 231–241.
- McDonough, W.F., 1990. Constraints on the composition of the continental lithospheric mantle. Earth Planet. Sci. Lett. 101, 1–18.
- McGetchin, T.R., Nikhanj, Y.S., Chodos, A.A., 1973. Carbonatite-kimberlite relations in the Cane Valley diatreme, San Juan County, Utah. J. Geophys. Res. 78, 1854–1869.
- McMillan, N.J., Dickin, A.P., Haag, D., 2000. Evolution of magma source regions in the Rio Grande rift, southern New Mexico. GSA Bull. 112 (10), 1582–1593.
- Michel, A., Villemant, B., 2003. Determination of halogens (F, Cl, Br, I), sulfur and water in seventeen geological reference materials. J. Geostand. Geoanalysis 27, 163–171.
- Naif, S., Key, K., Constable, S., Evans, R.L., 2015. Water-rich bending faults at the Middle America Trench. Geochem. Geophys. Geosyst. 16, 2582–2597.
- Patiño Douce, A.E., Roden, M.F., Chaumba, J., Fleisher, C., Yogodzinski, G., 2011. Compositional variability of terrestrial mantle apatites, thermodynamic modeling of apatite volatile contents, and the halogen and water budgets of planetary mantles. Chem. Geol. 288, 14–31.
- Pearson, D.G., Nowell, G.M., 2002. The continental lithospheric mantle: characteristics and significance as a mantle reservoir. Phil. Trans. R. Soc. Lond. A 360, 2383–2410.
- Perkins, G.B., Sharp, Z.D., Selverstone, J., 2006. Oxygen isotope evidence for subduction and rift-related mantle metasomatism beneath the Colorado Plateau-Rio Grande rift transition. Contrib. Mineral. Petrol. 151, 633–650.
- Ranero, C.R., Phipps Morgan, J., McIntosh, K., Reichert, C., 2003. Bending-related faulting and mantle serpentinization at the Middle America trench. Nature 425, 367–373.
- Rizzo, A.L., Faccini, B., Casetta, F., Faccincani, L., Ntaflos, T., Italiano, F., Coltorti, M., 2021. Melting and metasomatism in West Eifel and Siebengebirge Sub-Continental Lithospheric Mantle: Evidence from concentrations of volatiles in fluid inclusions and petrology of ultramafic xenoliths. Chem. Geol. 581, 120400.
- Roden, M., 1981. Origin of coexisting minette and ultramafic breccia, Navajo volcanic field. Contrib. Mineral. Petrol. 77, 195–206.
- Roden, M.F., Smith, D., Murthy, V.R., 1990. Chemical constraints on lithosphere composition and evolution beneath the Colorado Plateau. J. Geophys. Res. 95, 2811–2831.
- Rose-Koga, E.F., Koga, K.T., Moreira, M., Vlastelic, I., Jackson, M.G., Whitehouse, M.J., Shimizu, N., Habib, N., 2017. Geochemical systematics of Pb isotopes, fluorine, and sulfur in melt inclusions from São Miguel. Azores. Chem. Geol. 458, 22–37.
- Rowe, M.C., Lassiter, J.C., 2009. Chlorine enrichment in central Rio Grande Rift basaltic melt inclusions: Evidence for subduction modification of the lithospheric mantle. Geology 37 (5), 439–442.
- Rowe, M.C., Lassiter, J.C., Goff, K., 2015. Basalt volatile fluctuations during continental rifting: An example from the Rio Grande Rift, USA. Geochem. Geophys. Geosyst. 16, 1254–1273.
- Saal, A.E., Hauri, E.H., Langmuir, C.H., Perfit, M.R., 2002. Vapour undersaturation in primitive mid-ocean-ridge basalt and the volatile content of the Earth's upper mantle. Nature 419, 451–455.
- Salters, V.J.M., Stracke, A., 2004. Composition of the depleted mantle. Geochem. Geophys. Geosyst. 5, Q05B07.
- Scambelluri, M., Müntener, O., Ottolini, L., Pettke, T.T., Vannucci, R., 2004. The fate of B, Cl and Li in the subducted oceanic mantle and in the antigorite breakdown fluids. Earth Planet. Sci. Lett. 222, 217–234.
- Schilling, J.-G., Bergeron, M.B., Evans, R., 1980. Halogens in the mantle beneath the North Atlantic. Phil. Trans. R. Soc. Lond. A 297, 147–178.
- Schmidt, M.W., Poli, S., 1998. Experimentally based water budgets for dehydrating slabs and consequences for arc magma generation. Earth Planet. Sci. Lett. 163, 361–379.

- Schnetger, B., Muramatsu, Y., 1996. Determination of halogens, with special reference to iodine, in geological and biological samples using pyrohydrolysis for preparation and inductively coupled plasma mass spectrometry and ion chromatography for measurement. Analyst 121, 1627–1631.
- Sekimoto, S., Ebihara, M., 2016. Accurate Determination of Chlorine, Bromine and Iodine in U.S. Geological Survey Geochemical Reference Materials by Radiochemical Neutron Activation Analysis. Geostandards Geoanal. Res. 41 (2), 213–219.
- Sharp, Z.D., 1990. A laser-based microanalytical method for the in situ determination of oxygen isotope ratios of silicates and oxides. Geochim. Cosmochim. Acta 54, 1353–1357.
- Sharp, Z.D., Barnes, J.D., 2004. Water soluble chlorides in massive seafloor serpentinites: a source of chloride in subduction zones. Earth Planet. Sci. Lett. 226, 243–254.
- Sharp, Z.D., Draper, D.S., 2013. The chlorine abundance of Earth: Implications for a habitable planet. Earth Planet. Sci. Lett. 369, 71–77.
- Shaw, A.M., Behn, M.D., Humphris, S.E., Sohn, R.A., Gregg, P.M., 2010. Deep pooling of low degree melts and volatile fluxes at the 85°E segment of the Gakkel Ridge: evidence from olivine-hosted melt inclusions and glasses. Earth Planet. Sci. Lett. 289, 311–322.
- Shimizu, K., Suzuki, K., Saitoh, M., Konno, U., Kawagucci, S., Ueno, Y., 2015. Simultaneous determinations of fluorine, chlorine, and sulfur in rock samples by ion chromatography combined with pyrohydrolysis. Geochem. J. 49, 113– 124
- Shimizu, K., Saal, A.E., Myers, C.E., Nagle, A.N., Hauri, E.H., Forsyth, D.W., Kamenetsky, V.S., Niu, Y., 2016. Two-component mantle melting-mixing model for the generation of mid-ocean ridge basalts: Implications for the volatile content of the Pacific upper mantle. Geochim. Cosmochim. Acta 176, 44–80.
- Simons, K., Dixon, J.E., Schilling, J.-G., Kingsley, R., Poreda, R., 2002. Volatiles in basaltic glasses from the Easter-Salas y Gomez Seamount Chain and Easter Microplate: Implications for geochemical cycling of volatile elements. Geochem. Geophys. Geosyst. 3 (7).
- Smith, D., 1979. Hydrous minerals and carbonates in peridotite inclusions from Green Knobs and Buell Park kimberlitic diatremes on the Colorado Plateau. In: Boyd, F.R., Meyer, H.O.A. (Eds.), The Mantle Sample: Inclusions in Kimberlites and other Volcanics. American Geophysical Union, Washington D.C, pp. 345– 356.
- Smith, D., 1995. Chlorite-rich ultramafic reaction zones in Colorado Plateau xenoliths: recorders of sub-Moho hydration. Contrib. Mineral. Petrol. 121, 185–200.
- Smith, D., 2000. Insights into the evolution of the uppermost continental mantle from xenolith localities on and near the Colorado Plateau and regional comparisons. J. Geophys. Res. 105, 16769–16781.
- Smith, D., 2010. Antigorite Peridotite, Metaserpentinite, and other Inclusions within Diatremes on the Colorado Plateau, SW USA: Implications for the Mantle Wedge during Low-angle Subduction. J. Pet. 51, 1355–1379.
- Smith, D., 2013. Olivine thermometry and source constraints for mantle fragments in the Navajo Volcanic Field, Colorado Plateau, southwest United States: Implications for the mantle wedge. Geochem. Geophys. Geosyst. 14, 693–711.
- Smith, D., Levy, S., 1976. Petrology of the Green Knobs diatreme and implications for the upper mantle below the Colorado Plateau. Earth Planet. Sci. Lett. 29, 107– 125.

- Stracke, A., Snow, J.E., Hellebrand, E., von der Handt, A., Bourdon, B., Birbaum, K., Günther, D., 2011. Abyssal peridotite Hf isotopes identify extreme mantle depletion. Earth Planet. Sci. Lett. 308, 359–368.
- Straub, S.M., Layne, G.D., 2003. The systematics of chlorine, fluorine, and water in Izu arc front volcanic rocks: implications for volatile recycling in subduction zones. Geochim. Cosmochim. Acta 67 (21), 4179–4203.
- Sun, W.D., Binns, R.A., Fan, A.C., Kamenetsky, V.S., Wysoczanski, R., Wei, G.J., Hu, Y. H., Arculus, R.J., 2007. Chlorine in submarine volcanic glasses from the eastern Manus basin. Geochim. Cosmochim. Acta 71, 1542–1552.
- Svensen, H., Jamtveit, B., Banks, D.A., Austrheim, H., 2001. Halogen contents of eclogite facies fluid inclusions and minerals: Caledonides, western Norway. J. Metamorph. Geol. 19, 165–178.
- Thompson, R.N., Ottley, C.J., Smith, P.M., Pearson, D.G., Dickin, A.P., Morrison, M.A., Leat, P.T., Gibson, S.A., 2005. Source of the Quaternary Alkalic Basalts, Picrites and Basanites of the Potrillo Volcanic Field, New Mexico, USA: Lithosphere or Convecting Mantle? J. Petrol. 46 (8), 1603–1643.
- Toyama, C., Sumino, H., Okabe, N., Ishikawa, A., Yamamoto, J., Kaneoka, I., Muramatsu, Y., 2021. Halogen heterogeneity in the subcontinental lithospheric mantle revealed by I/Br ratios in kimberlites and their mantle xenoliths from South Africa, Greenland, China, Siberia, Canada, and Brazil. Amer. Mineral. 106, 1890–1899.
- Ulmer, P., Trommsdorff, V., 1995. Serpentine stability to mantle depths and subduction-related magmatism. Science 268, 858–861.
- Urann, B.M., Le Roux, V., Hammond, K., Marschall, H.R., Lee, C.-T.-A., Monteleone, B. D., 2017. Fluorine and chlorine in mantle minerals and the halogen budget of the Earth's mantle. Contrib. Mineral. Petrol. 172, 51.
- Urann, B.M., Le Roux, V., John, T., Beaudoin, G.M., Barnes, J.D., 2020. The distribution and abundance of halogens in eclogites: An in-situ SIMS perspective of the Raspas Complex (Ecuador). Am. Mineral. 105, 307–318.
- Valley, J.W., Kitchen, N., Kohn, M.J., Niendorf, C.R., Spicuzza, M.J., 1995. UWG-2, a garnet standard for oxygen isotope ratios: Strategies for high precision and accuracy with laser heating. Geochim. Cosmochim. Acta 59, 5223–5231.
- Waelkens, C.M., Stix, J., Monteleone, B., Burckel, P., 2021. Efficient release of bromine by super-eruptions. Geology 49, 1416–1420.
- Wedepohl, K.H., Gohn, E., Hartmann, G., 1994. Cenozoic alkali basaltic magmas of western Germany and their products of differentiation. Contrib. Mineral. Petrol. 115. 253–278.
- Wenner, D.B., Taylor, H.P., 1973. Oxygen and hydrogen isotope studies of the serpentinization of ultramafic rocks in oceanic environments and continental ophiolite complexes. Am. J. Sci. 273, 207–239.
- West, M., Ni, J., Baldridge, W.S., Wilson, D., Aster, R., Gao, W., Grand, S., 2004. Crust and upper mantle shear wave structure of the southwest United States: Implications for rifting and support for high elevation. J. Geophys. Res. 109, 803309
- Witt-Eickschen, G., Seck, H.A., Mezger, K., Eggins, S.M., Altherr, R., 2003. Lithospheric Mantle Evolution beneath the Eifel (Germany): Constraints from Sr-Nd-Pb Isotopes and Trace Element Abundances in Spinel Peridotite and Pyroxenite Xenoliths. J. Pet. 44 (6), 1077–1095.
- Workman, R.K., Hart, S.R., 2005. Major and trace element composition of the depleted MORB mantle (DMM). Earth Planet. Sci. Lett. 231 (1–2), 53–72.
- Workman, R.K., Hauri, E.H., Hart, S.R., Wang, J., Blusztajn, J., 2006. Volatile and trace elements in basaltic glasses from Samoa: implications for water distribution in the mantle. Earth Planet. Sci. Lett. 241, 932–951.